

# **8. PHYSICS ISSUES FOR COMPACT REVERSED-FIELD-PINCH REACTORS**

Robert A. Krakowski

Farrokh Najmabadi

## Contents

8.1.	INTRODUCTION . . . . .	8-1
8.2.	CONFINEMENT . . . . .	8-8
8.2.1.	Reactor Conditions . . . . .	8-8
8.2.2.	Physics Data Base . . . . .	8-10
8.2.3.	Reactor Implications . . . . .	8-18
8.3.	CURRENT DRIVE . . . . .	8-21
8.3.1.	Reactor Conditions . . . . .	8-22
8.3.2.	Physics Data Base . . . . .	8-22
8.3.3.	Reactor Implications . . . . .	8-25
8.4.	IMPURITY CONTROL . . . . .	8-28
8.4.1.	Reactor Conditions . . . . .	8-28
8.4.2.	Physics Data Base . . . . .	8-30
8.4.3.	Reactor Implications . . . . .	8-32
8.5.	FORMATION AND START-UP . . . . .	8-36
8.5.1.	Reactor Conditions . . . . .	8-36
8.5.2.	Physics Data Base . . . . .	8-37
8.5.3.	Reactor Implications . . . . .	8-47
8.6.	SUMMARY AND RECOMMENDATIONS . . . . .	8-51
	REFERENCES . . . . .	8-53

## 8. PHYSICS ISSUES FOR COMPACT REVERSED-FIELD-PINCH REACTORS

### 8.1. INTRODUCTION

The TITAN research program is a multi-institutional [1] effort to determine the potential of the reversed-field-pinch (RFP) magnetic fusion concept as a compact, high-power-density, and “attractive” fusion energy system from economics (cost of electricity, COE), safety, environmental, and operational viewpoints.

In recent reactor studies, the compact reactor option [2-5] has been identified as one approach toward a more affordable and competitive fusion reactor. The main feature of a compact reactor is a fusion power core (FPC) with a mass power density in excess of 100 to 200 kWe/tonne. Mass power density (MPD) is defined [2] as the ratio of the net electric power to the mass of the FPC, which includes the plasma chamber, first wall, blanket, shield, magnets, and related structure. The increase in MPD is achieved by increasing the plasma power density and neutron wall loading, by reducing the size and mass of the FPC through decreasing the blanket and shield thicknesses and using resistive magnet coils, as well as by increasing the blanket energy multiplication. A compact reactor, therefore, strives toward a system with an FPC comparable in mass and volume to the heat sources of alternative fission power plants, with MPDs ranging from 500 to 1000 kWe/tonne and competitive cost of energy.

Other potential benefits for compact systems can be envisaged in addition to improved economics. The FPC cost in a compact reactor is a small portion of the plant cost and, therefore, the economics of the reactor will be less sensitive to changes in the unit cost of FPC components or the plasma performance. Moreover, since a high-MPD FPC is smaller and cheaper, a rapid development program at lower cost should be possible, changes in the FPC design will not introduce large cost penalties, and the economics of learning curves can be readily exploited throughout the plant life.

The RFP has inherent characteristics which allow it to operate at very high mass power densities. This potential is available because the main confining field in an RFP is the poloidal field, which is generated by the large toroidal current flowing in the plasma. This feature results in a low field at the external magnet coils, a high plasma beta, and a very high engineering beta (defined as the ratio of the plasma pressure to the square

of the magnetic field strength at the coils) as compared to other confinement schemes. Furthermore, sufficiently low magnetic field at the external coils permits the use of normal coils while joule losses remain a small fraction of the plant output. This option allows a thinner blanket and shield. In addition, the high current density in the plasma allows ohmic heating to ignition, eliminating the need for auxiliary heating equipment. Also, the RFP concept promises the possibility of efficient current-drive systems based on low-frequency oscillations of poloidal and toroidal fluxes and the theory of RFP relaxed states. The RFP confinement concept allows arbitrary aspect ratios, and the circular cross section of plasma eliminates the need for plasma shaping coils. Lastly, the higher plasma densities particularly at the edge, together with operation with a highly radiative RFP plasma, significantly reduce the divertor heat flux and erosion problems.

These inherent characteristics of the RFP [6] allow it to meet, and actually far exceed, the economic threshold MPD value of 100 kWe/tonne. As a result, the TITAN study also seeks to find potentially significant benefits and to illuminate main drawbacks of operating well above the MPD threshold of 100 kWe/tonne. The program, therefore, has chosen a minimum cost, high neutron wall loading of  $18 \text{ MW/m}^2$  as the reference case in order to quantify the issue of engineering practicality of operating at high mass power densities. The TITAN study has also put strong emphasis on safety and environmental features in order to determine if high-power-density reactors can be designed with a high level of safety assurance and with low-activation material to qualify for Class-C waste disposal.

An important potential benefit of operating at a very high MPD is that the small physical size and mass of a compact reactor permits the design to be made of only a few pieces and a single-piece maintenance approach will be feasible [7,8]. Single-piece maintenance refers to a procedure in which all of components that must be changed during the scheduled maintenance are replaced as a single unit, although the actual maintenance procedure may involve the movement, storage, and reinstallation of some other reactor components. In TITAN designs, the entire reactor torus is replaced as a single unit during the annual scheduled maintenance. The single-piece maintenance procedure is expected to result in the shortest period of downtime during the scheduled maintenance period because: (1) the number of connects and disconnects needed to replace components will be minimized; and (2) the installation time is much shorter because the replaced components are pretested and aligned as a single unit before commitment to service. Furthermore, recovery from unscheduled events will be more standard and rapid because complete components will be replaced and the reactor brought back on line. The repair work will then be performed outside the reactor vault.

To demonstrate the possibility of multiple engineering approaches to the high-power-density option, the TITAN study has developed two FPC embodiments: TITAN-I, a self-cooled liquid-lithium-metal loop design with vanadium-alloy structure, and TITAN-II, a self-cooled aqueous-lithium-salt pool design with ferritic-steel structure.

The operating space of a compact RFP reactor has been examined using a comprehensive parametric systems model which includes the evolving state of knowledge of the physics of RFP confinement and embodies the TITAN-I and TITAN-II engineering approaches (Section 3). Two key figures of merit, the cost of electricity (COE) and mass power density (MPD), are monitored by the parametric systems model and are displayed in Figure 8.1-1 as functions of the neutron wall loading. Figure 8.1-1 shows that the COE is relatively insensitive to wall loadings in the range of 10 to 20 MW/m<sup>2</sup>, with a shallow minimum at about 19 MW/m<sup>2</sup>. The MPD is found to increase monotonically with the

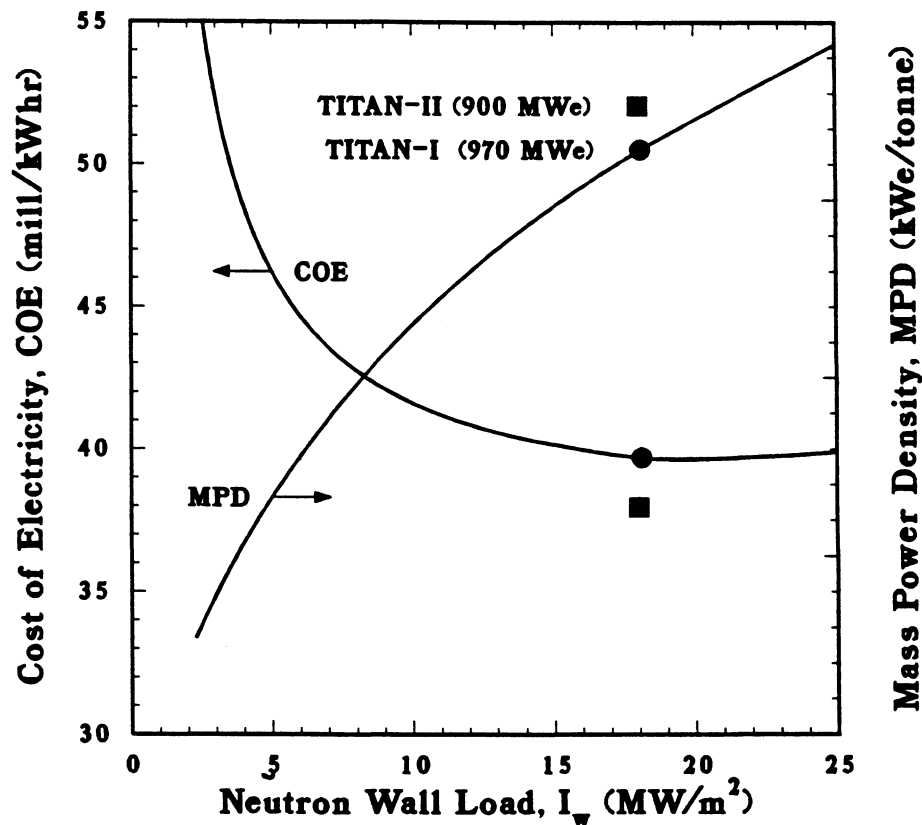


Figure 8.1-1. The COE and MPD as functions of neutron wall loading for the TITAN-class RFP reactors. TITAN-I (filled circle) and TITAN-II (filled squares) reference design points are also shown.

wall load. For designs with a neutron wall load larger than about  $10 \text{ MW/m}^2$ , the FPC is physically small enough such that single-piece FPC maintenance is feasible. These considerations point to a design window for compact RFP reactors with neutron wall loading in the range of 10 to  $20 \text{ MW/m}^2$ . The TITAN-class RFP reactors in this design window have an MPD in excess of  $500 \text{ kWe/tonne}$ , and an FPC engineering power density in the range of 5 to  $15 \text{ MWt/m}^3$ ; these values represent improvements by factors of 10 to 30 compared with earlier fusion reactor designs. The FPC cost is a smaller portion of the total plant cost (typically about 12%) compared with 25% to 30% for earlier RFP designs [4,5]. Therefore, the unit direct cost (UDC) is less sensitive to related physics and technology uncertainties.

Near-minimum-COE TITAN-I and TITAN-II design points, incorporating distinct blanket thermal-hydraulic options, materials choices, and neutronics performances have been identified in Figure 8.1-1. The major parameters of the TITAN reactors are summarized in Table 8.1-I. The engineering analyses of TITAN-I and TITAN-II FPCs are presented, respectively, in Sections 9 through 14 and Sections 15 through 20. The parameters of the TITAN reference design points, based on detailed subsystem design, are included in Appendices A and B and follow the DOE/OFE standard reporting format. Appendices also include cost tables and parametric systems code predictions of subsystem parameters for comparison with DOE/OFE tables.

In order to permit a comparison, the TITAN reference design points have similar plasma parameters and wall loadings allowing for certain plasma engineering analyses to be common between the two designs. Major physics features of the TITAN designs are summarized in Table 8.1-II.

One of the major objectives of the TITAN study is to identify and assess the physics requirements of high-MPD RFP reactors. The experimental and theoretical bases for RFPs have grown rapidly during the last few years [6], but a large degree of extrapolation to TITAN-class reactors is still required (Table 8.1-III). The degree of extrapolation is one to two orders of magnitude in plasma current and temperature and two to three orders of magnitude in energy confinement time. However, the TITAN plasma density, poloidal beta, and plasma current density all are close to present-day experimental achievements. The next generation of RFP experiments [9,10] with hotter plasmas will extend the data base toward reactor-relevant regimes of operation. The TITAN study has brought out and illuminated a number of key physics issues, some of which require greater attention from the RFP physics community.

The physics of confinement scaling, plasma transport, RFP plasma formation and start-up, and the role of the conducting shell are already major efforts in RFP research.

**Table 8.1-I.**  
**OPERATING PARAMETERS OF TITAN FUSION POWER CORES**

	TITAN-I	TITAN-II
Major radius (m)	3.9	3.9
Minor plasma radius (m)	0.60	0.60
First wall radius (m)	0.66	0.66
Plasma current (MA)	17.8	17.8
Toroidal field on plasma surface (T)	0.36	0.36
Poloidal beta	0.23	0.23
Neutron wall load (MW/m <sup>2</sup> )	18	18
Radiation heat flux on first wall (MW/m <sup>2</sup> )	4.6	4.6
Primary coolant	Liquid lithium	Aqueous solution
Structural material	V-3Ti-1Si	Ferritic steel 9-C
Breeder material	Liquid lithium	LiNO <sub>3</sub>
Neutron multiplier	none	Be
Coolant inlet temperature (°C)	320	298
First-wall-coolant exit temperature (°C)	440	330
Blanket-coolant exit temperature (°C)	700	330
Coolant pumping power (MW)	48	49
Fusion power (MW)	2301	2290
Total thermal power (MW)	2935	3027
Net electric power (MW)	970	900
Gross efficiency	44%	35%
Net efficiency	33%	30%
Mass power density, MPD (kWe/tonne)	757	806
Cost of electricity, COE (mill/kWh)	39.7	38.0

Table 8.1-II.

## PHYSICS FEATURES OF TITAN REACTORS

- 
- Confinement scaling:  $\tau_{E_e} \propto I_\phi^\nu r_p^2 f(\beta_\theta)$  with a soft beta limit;
  - Poloidal beta:  $\beta_\theta \simeq 0.22$ , including energetic alpha particles;
  - Radiation-dominated plasma:  $f_{RAD} \simeq 0.96$  for the combined core and edge plasma;
  - Poloidally symmetric, toroidal-field divertors for impurity control and particle exhaust;
  - Current drive using oscillating-field helicity injection;
  - Shell stabilization for  $\leq 10$  ms;
  - Relaxation-assisted start-up and sustainment;
  - Density and field control of current terminations;
  - Open poloidal-field-coil configuration with superconducting equilibrium-field coils;
  - Bipolar start-up with low back-bias toroidal field.
- 

However, the TITAN study points to three other major issues. First, operating high-power-density fusion reactors with intensely radiating plasmas is crucial. Confirming that the global energy confinement time remains relatively unaffected while core-plasma radiation increases (a possible unique feature of RFP) is extremely important. Second, the TITAN study has adopted the use of three “open-geometry” toroidal divertors as the impurity-control and particle-exhaust system. Even with an intensely radiative plasma, using an array of poloidal pump-limiters as the impurity-control system would suffer from the serious erosion of the limiter blades (and possibly the first wall). The physics of toroidal-field divertors in RFPs must be examined, and the impact of the magnetic separatrix on RFP confinement must be studied. If toroidal divertors are consistent with confinement and stability in RFPs, then high-recycling divertors and the predicted

**Table 8.1-III.**  
**PARAMETERS OF MAJOR RFP DEVICES**

Device	Major Radius (m)	Minor Radius (m)	Plasma Current (MA)	Current Density (MA/m <sup>2</sup> )	Electron Temperature (keV)	Average Density (10 <sup>20</sup> m <sup>-3</sup> )	Poloidal Beta
TPE-1RM <sup>(a)</sup>	0.50	0.09	0.13	5.1	0.60	0.3	0.1
ETA-BETA-II <sup>(b)</sup>	0.65	0.125	0.15	3.0	0.08	1.0	0.1
HBTX1A <sup>(c)</sup>	0.80	0.26	0.32	1.5	0.10	0.2	0.05
OHTE/RFP <sup>(d)</sup>	1.24	0.20	0.50	4.5	0.4 - 0.6	0.5 - 3.0	0.1 - 0.2
ZT-40M <sup>(e)</sup>	1.14	0.20	0.44	3.5	0.3 - 0.5	0.4 - 0.9	0.1 - 0.2
RFX <sup>(f)</sup>	2.00	0.48	2.0	2.8	0.5 - 2.0	0.3 - 2.0	0.10
CPRF/ZTH <sup>(g)</sup>	2.40	0.40	4.0	8.0	0.5 - 5.0	0.3 - 5.0	0.10
FTF/RFP <sup>(h)</sup>	1.80	0.30	10.4	37.	10. - 20.	6.0 - 9.0	0.1 - 0.2
TITAN <sup>(i)</sup>	3.80	0.60	18.2	16.	10. - 20.	9.0	0.2

(a) Existing experiment at ETL, Japan [11].

(b) Existing experiment at Padova, Italy [12].

(c) Existing experiment at Culham, U. K. [13].

(d) Existing experiment at General Atomics, U. S. A. [14].

(e) Existing experiment at Los Alamos National Laboratory, U. S. A. [15].

(f) Planned experiment at Padova, Italy [10,16].

(g) Planned experiment at Los Alamos National Laboratory, U. S. A. [9,16].

(h) Conceptual neutron source, a Los Alamos National Laboratory study, U. S. A. [17].

(i) Conceptual reactor design, a UCLA-led multi-institutional study, U. S. A.

high-density, low-temperature scrape-off layer must be also confirmed. Third, early work in the TITAN study convinced the team that high-MPD, compact RFP reactors must operate at steady state. Current drive by magnetic helicity injection utilizing the natural relaxation process in RFP plasma is predicted to be efficient [18,19] but experiments on oscillating-field current drive (OFCD) are inconclusive. Testing OFCD in higher temperature plasmas must await the next generation of RFP experiments, namely ZTH [9,16] and RFX [10,16].

The key physics issues of confinement, impurity control, current drive, and RFP formation and start-up are reviewed in detail in Sections 8.2 through 8.5, respectively. These issues are to varying degrees interrelated and, therefore, interfaces and connections are identified when appropriated. For each physics issue, the TITAN reactor requirements and the present physics data base are reviewed in order to identify those high-leverage areas that require further experimental and theoretical work. The sensitivity of the reactor performance to these physics assumptions and extrapolation have also been studied using the parametric systems code.

## 8.2. CONFINEMENT

The physics issues related to plasma confinement include: (1) energy and particle confinement in a plasma with dynamo-related turbulence, (2) the magnitude and scaling of the normalized plasma pressure,  $\beta_\theta$ , and (3) the degree to which the plasma can shed energy by radiation as opposed to intrinsic transport channels without impacting the global confinement. These confinement issues should be addressed for both ohmic-heated and alpha-particle-heated discharges.

### 8.2.1. Reactor Conditions

As for most fusion reactor designs, the specifications of the net-electric power (*i.e.*, total fusion power,  $P_F$ ), plasma power balance (*i.e.*,  $n\tau_E T$ ), and neutron wall loading,  $I_w$ , give the global energy confinement time,  $\tau_E \propto (P_F/A)^{1/4} (n\tau_E T)/I_w^{3/4}$ . The value of neutron wall loading is determined by the minimization of COE in TITAN, therefore, the above value of  $\tau_E$  represent an “economic” confinement time,  $\tau_E(\text{ECON})$ , which must be compared with experimental predictions,  $\tau_E(\text{PHYS})$ . The economic confinement required to achieve the minimum-COE design point for TITAN (Figure 8.1-1) is  $\tau_E(\text{ECON}) = 0.22 \text{ s}$ , or  $\chi_E = 0.32 \text{ m}^2/\text{s}$ . For TITAN, this level of global energy confinement must be attained in a highly radiating core plasma (with a radiation fraction,

$f_{RAD}^c \simeq 0.7$ ) with a poloidal beta,  $\beta_\theta = 0.22$  (including a beta increment of  $\sim 0.02$  for energetic alpha particles).

A simplified energy balance for a non-radiating, ohmically heated plasma gives

$$\tau_E = \frac{3\mu_o}{16} \frac{\beta_\theta r_p^2}{\eta}, \quad (8.2-1)$$

where  $\eta$  is the effective plasma resistivity. Under conditions of constant  $\beta_\theta$  and  $j_\phi/n$ , pressure balance gives  $T \propto I_\phi$ , and for a classical scaling of resistivity with temperature ( $\eta \propto T^{-3/2}$ ) results in  $\tau_{Ee} \propto I_\phi^\nu r_p^2$  with  $\nu = 1.5$ . Any variations from these assumptions as well as variations in profile factors, impurity concentration, and  $Z_{eff}$ , will alter the dependence of  $\tau_E$  on  $I_\phi$  and  $r_p$ . Until experiment data on the plasma profiles and  $Z_{eff}$  become available, the expression  $\tau_{Ee} \propto C_\nu I_\phi^\nu r_p^2$  is used to parametrically fit the existing experimental data.

The TITAN systems code, as well as the plasma engineering effort, has used a physics scaling of the form  $\tau_E(\text{PHYS}) = 2(1/\tau_{Ee} + 1/\tau_{Ei})^{-1}$  with  $\tau_{Ee} = C_\nu I_\phi^\nu r_p^2 f(\beta_\theta)$  and  $\tau_{Ei} \simeq 4\tau_{Ee}$ . The current exponent  $\nu = 0.8$  to  $1.5$  represents a range of fits to the global confinement observed in experiments after corrections for radiative loss have been applied. The function  $f(\beta_\theta)$  reflects an attempt to model a beta limit that may exist in RFPs with  $f(\beta_\theta) = 1$  for low values of  $\beta_\theta$  and  $f(\beta_\theta) \rightarrow 0$  when  $\beta_\theta$  exceeds a critical value of beta, thereby giving considerable thermal stability to the burn.

Several important points should be noted: (1) The above empirical scaling is derived from experiments with limited variations in both  $I_\phi$  and  $r_p$ . (2) In the present ohmically heated discharges,  $\beta_\theta$  and  $\tau_E$  (or  $\chi_E$ ) are inexorably coupled and it is not clear that the above empirical scaling of confinement will be applicable to fusion discharges where alpha-particle heating is dominant. (3) Zero-dimensional simulation of plasma start-up for TITAN reactors with the above scaling shows that the ignition is achieved at  $\beta_\theta \simeq 0.05-0.1$  ( $\tau_E \simeq 0.4$  s) and the value of  $\beta_\theta \simeq 0.22$  is only reached at the steady-state burn condition. Since the above scaling is derived for the flat-top portion of experimental discharges with  $\beta_\theta$  being close to its limit, applicability of this scaling to TITAN start-up simulations is questionable.

The level of field error, particularly as related to the size and formation of magnetic islands, must be sufficiently low to not adversely impact plasma confinement. The toroidal-field (TF) and divertor coils of TITAN reactors are designed such that the toroidal-field ripple is constrained to  $\Delta B_R/B_\theta \leq 0.03$ . As a result, the overall island widths are less than a quarter of the distance between the reversal surface and plasma (separatrix) surface; this annular region is assumed to be crucial for RFP confinement.

Table 8.2-I.

**IMPURITY CONCENTRATION AND RADIATION FRACTIONS  
IN THE TITAN PLASMA**

Location	$n_{Xe}$ ( $10^{18} \text{ m}^{-3}$ )	$n_i$ ( $10^{20} \text{ m}^{-3}$ )	$f_{RAD} = P_{RAD}/P_{TOT}^{(a)}$
Core	0.289	8.9	0.695
Edge	0.289	1.7	0.232
Divertor	10.50	62.0	0.039

(a)  $P_{TOT} = P_{OHM} + P_{\alpha} = 552 \text{ MW}$ .

One-dimensional (radial) plasma simulations were performed to determine achievable values of  $f_{RAD}^c$  for a given kind and quantity of injected impurity (Section 5.3). For these calculations, the local beta limit described above in terms of  $f(\beta_{\theta})$  is imposed. This limit enhances the local electron perpendicular thermal conductivity and the particle diffusivity by large factors above classical values, especially in the central plasma region when the on-axis beta exceeds a critical limit. For ohmically heated plasmas with small radiation losses, these assumptions lead to a global scaling of the form given above with  $\nu \simeq 1.5$ .

The 1-D plasma simulations were performed assuming a uniform impurity concentration and a coronal equilibrium model. The values of the core-plasma radiation fraction ( $f_{RAD}^c$ ) and the resultant  $Z_{eff}$  are estimated as functions of the impurity concentration for several impurity species and the results are given in Figure 8.2-1. High- $Z$  impurities are preferred because a high value of  $f_{RAD}^c$  can be achieved for minimum  $Z_{eff}$  (to minimize  $V_{\phi}$  and the OFCD requirements). Combined with similar estimates of the edge-plasma and divertor radiation fractions, a total radiation fraction of  $f_{RAD}^{TOT} = 0.97$  is possible for the Xe impurity concentrations given on Table 8.2-I.

### 8.2.2. Physics Data Base

The essential elements of the RFP experimental data base in the confinement area are: (1) scaling of plasma temperature and/or pressure with current (*i.e.*, confining

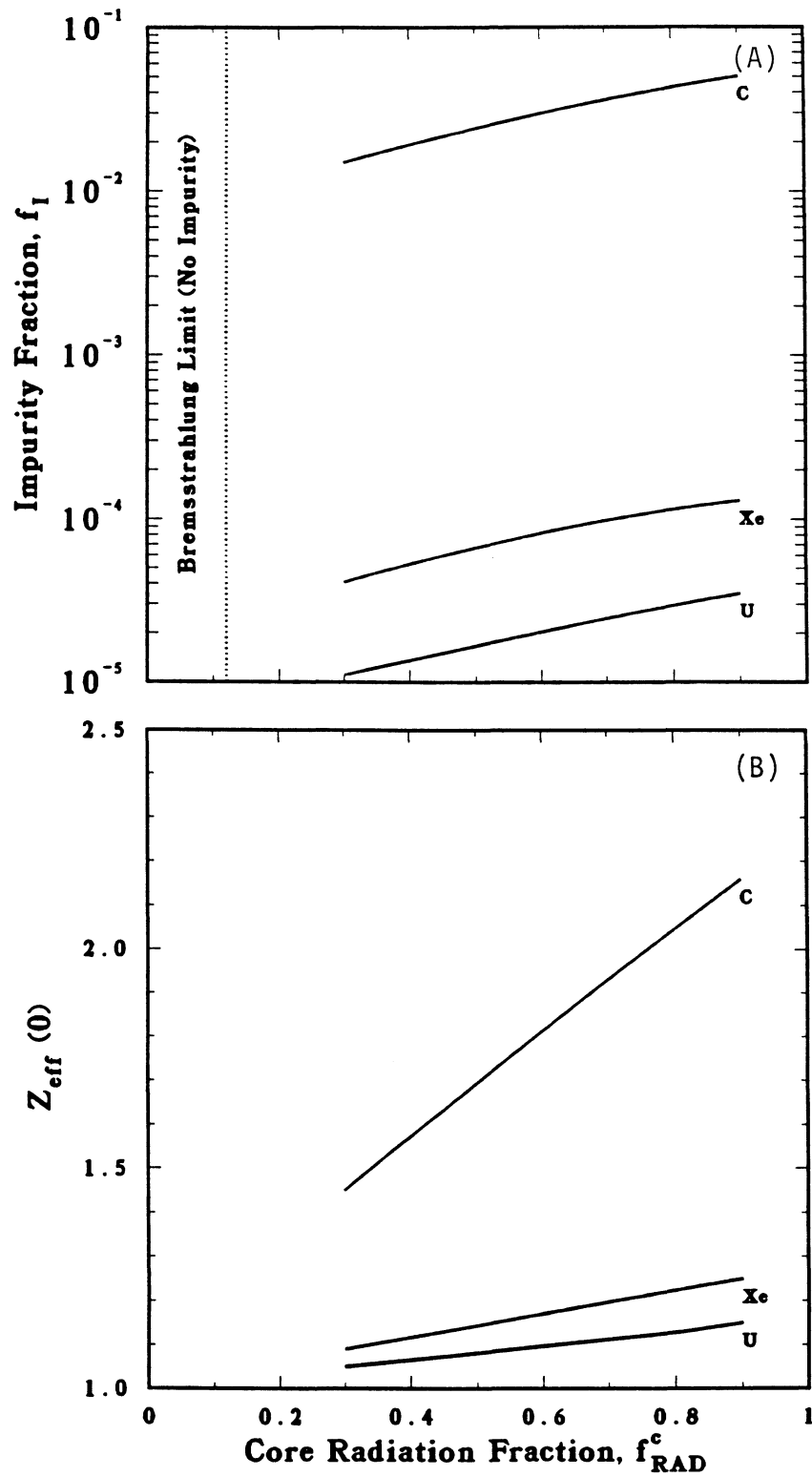


Figure 8.2-1. The required impurity fraction (A) and the resultant  $Z_{eff}$  (B) as functions of the core radiation fraction,  $f_{RAD}^c$ , for different impurities.

magnetic field); (2) scaling of plasma energy confinement with plasma current and size; and (3) partition of plasma energy loss between radiative and intrinsic (conduction and convection) channels. A more extensive review of the present data base is given in Section 2.3; only examples typical of desirable behavior are repeated here.

### 8.2.2.1. Temperature, density, and pressure scalings

Extensive measurements of the dependence of the plasma temperature on current for a range of RFPs indicate that the on-axis electron temperature increases with plasma current raised to a power in the range of 0.5-1.0. Temperature increases on the order of 1 eV/kA have been observed. Figures 8.2-2 and 8.2-3 show this behavior for the OHTE/RFP [14] and the ZT-40M [20] experiments. The ZT-40M data are for a range of conditions and show  $T_e(0) \propto I_\phi^{1.2}$  and  $n_e T_e(0) \propto I_\phi^2$  (*i.e.*, approximately constant  $\beta_\theta$  if  $T_e(0)/T_e$  is constant and  $T_i \simeq T_e$ ). In other experiments on ZT-40M with current flat-top operation and longer pulses, it was found that  $T_e(0) \propto I_\phi^{0.7}$ , but in these conditions  $n \propto I_\phi^{1.3}$ , again resulting in  $n_e T_e(0) \propto I_\phi^2$  and a constant-beta scaling.

More recent results from HBTX1A [12] and ZT-40M [21] suggest that the temperature-current scaling might be better described by postulating a constant beta, with a slope determined by  $I_\phi/N$ . Evidence from a number of experiments indicates that the maximum value of  $\beta_\theta$  varies relatively little over a range of conditions and from one machine to another. Some variation of  $\beta_\theta$  with  $I_\phi/N$  has been reported, with  $\beta_\theta$  increasing somewhat as  $I_\phi/N$  is reduced. It should also be noted that the range over which favorable scaling is obtained appears to be extended by improved wall-conditioning methods and by reduction in field errors [13].

### 8.2.2.2. Confinement scaling

Only limited confinement-scaling information for RFPs is available, and the variation of the main parameters, particularly geometry, is limited. Furthermore, all RFPs to date are only ohmically heated. The first recent estimates of energy confinement in RFPs have been made possible by the relatively stationary conditions achieved in flat-top current discharges. With the global energy confinement time,  $\tau_E$ , defined as plasma energy divided by the ohmic power and defining an effective global diffusivity as  $\chi_E = (3/16)r_p^2/\tau_E$ , it follows that in general  $\chi_E = \eta\beta_\theta/\mu_0$ . Depending on assumptions made with respect to the constancy of  $\beta_\theta$ ,  $j_\phi/n$ ,  $Z_{eff}$ , profiles, *etc.*, and the scaling of  $\eta$  with temperature

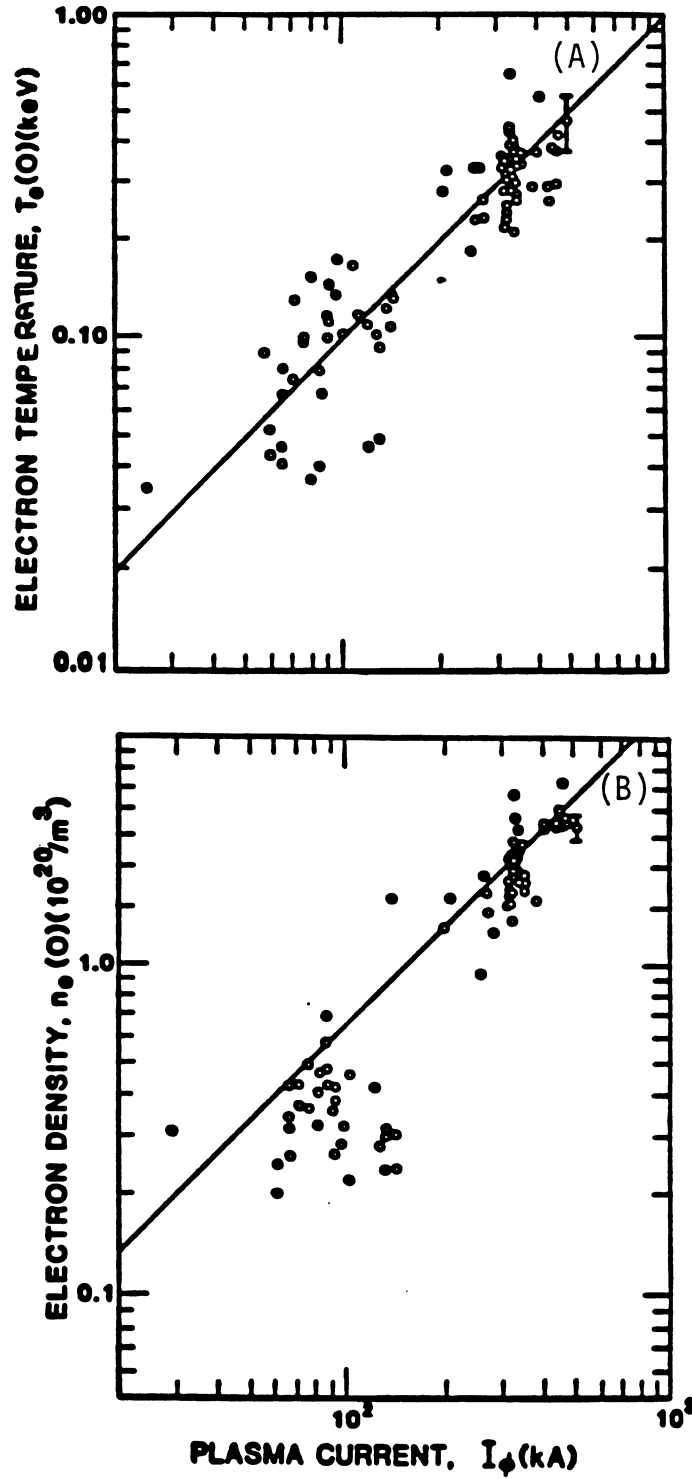


Figure 8.2-2. Variation of central electron temperature (A) and central electron density (B) with the plasma current for the OHTE/RFP experiment [14].

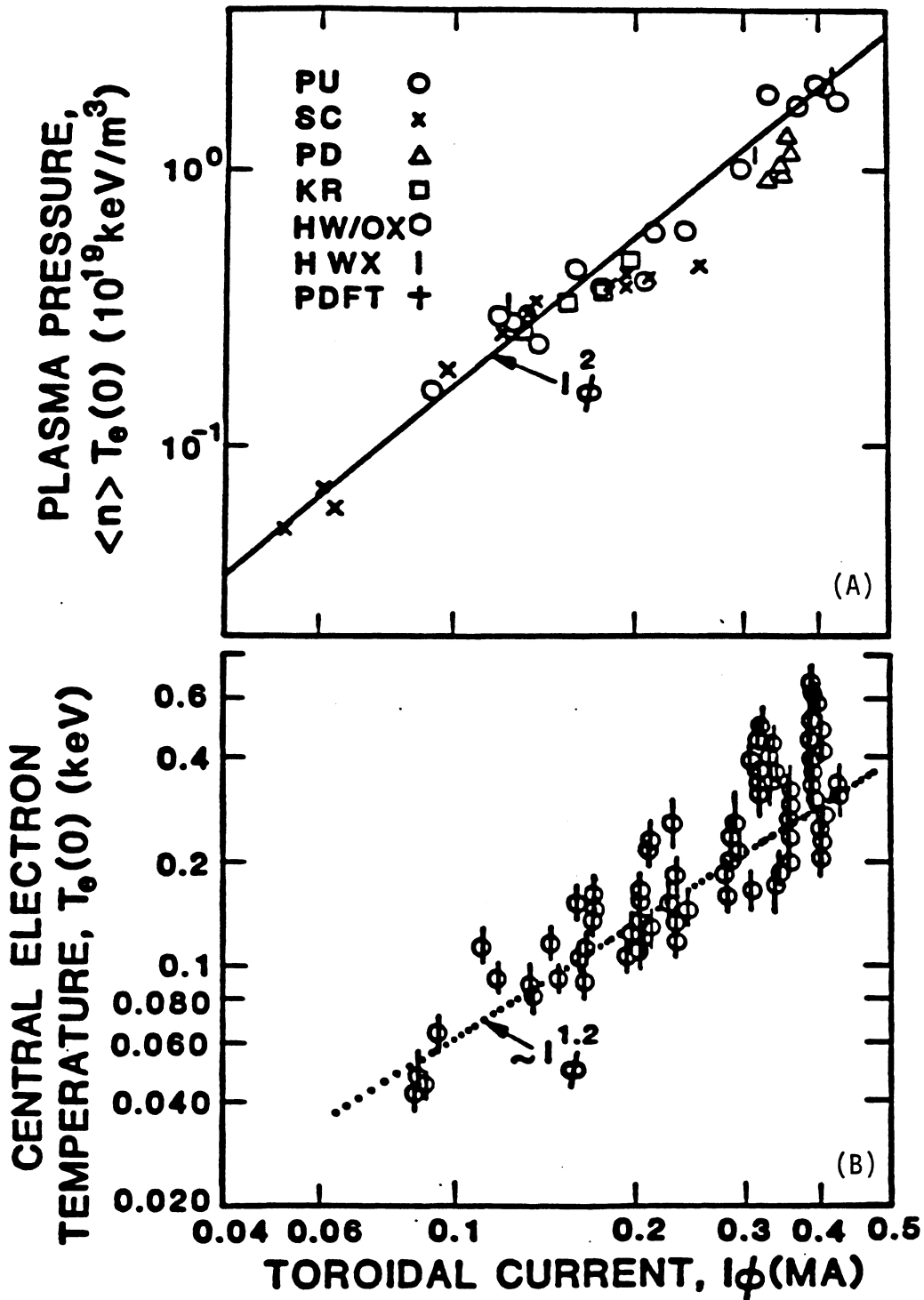


Figure 8.2-3. Variation of the product of central electron temperature with the average electron density (A) and the central electron temperature (B) with the plasma current for the ZT-40M experiment [20].

or current, a range of scaling of  $\chi_E$  with current, beta, and geometry can be derived. Assuming classical scaling for  $\eta$ , the definitions of  $\beta_\theta$  and  $\chi_E$  result in

$$1/\chi_E \propto (j_\phi/n)^{3/2} \beta_\theta^{5/2} I_\phi^{3/2} / Z_{eff}, \quad (8.2-2)$$

which for constant  $\beta_\theta$  and  $j_\phi/n$  predicts  $1/\chi_E \propto T_\phi^{3/2} / Z_{eff}$ . The inverse global diffusivity (corrected for radiative losses) is plotted in Figure 8.2-4 for a number of RFP experiments. Also shown on Figure 8.2-5 is the dependence of  $n\tau_E$  on  $I_\phi$  for ZT-40M [20], with the assumptions of constant  $\beta_\theta$  and  $j_\phi/n$  predicting  $n\tau_E \propto \beta_\theta^2 I_\phi^{5/2}$ .

Figures 8.2-4 and 8.2-5 represents the early RFP data base, an extension of which has been summarized in Section 2.3.5. As noted in that section, even more recent extensions of this data base indicate that the experimental beta (based on average density, but central electron temperature) may be decreasing somewhat with increasing current. This apparent decrease could be attributable to flattening temperature profiles or  $T_i > T_e$  in regions where  $I_\phi/N$  is increasing. Furthermore,  $\tau_E$  for a given device (again measured using average density and central electron temperature) may be increasing with current less rapidly than predicted by the simplified scaling relationships for  $\tau_E$  or  $\chi_E$  given above. These recent extensions of the RFP scaling data base generally represent increases in statistical breadth, with an emphasis placed on the lower-current ( $\sim 50$ -70 kA) regime. Increases in  $Z_{eff}$  and broadening of temperature profiles can explain these more recent projections. A clear resolution of these issues, however, must await higher-current experiments ( $> 0.5$  MA) that use improved  $Z_{eff}$  and profile diagnostics as well as stricter edge-plasma and density control. Until these issues are resolved by experiments presently being designed and built, an empirical scaling of the kind suggested above ( $\tau_E \propto I_\phi^2 r_p^2$ ) is parametrically applied to quantitatively express the main reactor requirements. These issues are addressed in more detail in Section 2.3.

### 8.2.2.3. Highly radiative RFP plasma

The scaling of plasma pressure with current observed in Figures 8.2-2 and 8.2-3 suggests a beta limit wherein intrinsic transport would adjust through changing MHD activity if other loss channels (*e.g.*, radiation) become available. Under this hypothesis, as the fraction of the total energy loss carried through the radiation channel,  $f_{RAD}^c = P_{RAD}/P_{OHM}$ , is increased, the non-radiative (*i.e.*, intrinsic) confinement time,  $\tau_E^{NR}$ , is expected to increase according to  $\tau_E/(1 - f_{RAD}^c)$ .

A preliminary test of this hypothesis that energy loss channels can be adjusted to maintain a constant plasma energy content was performed on ZT-40M by adding trace

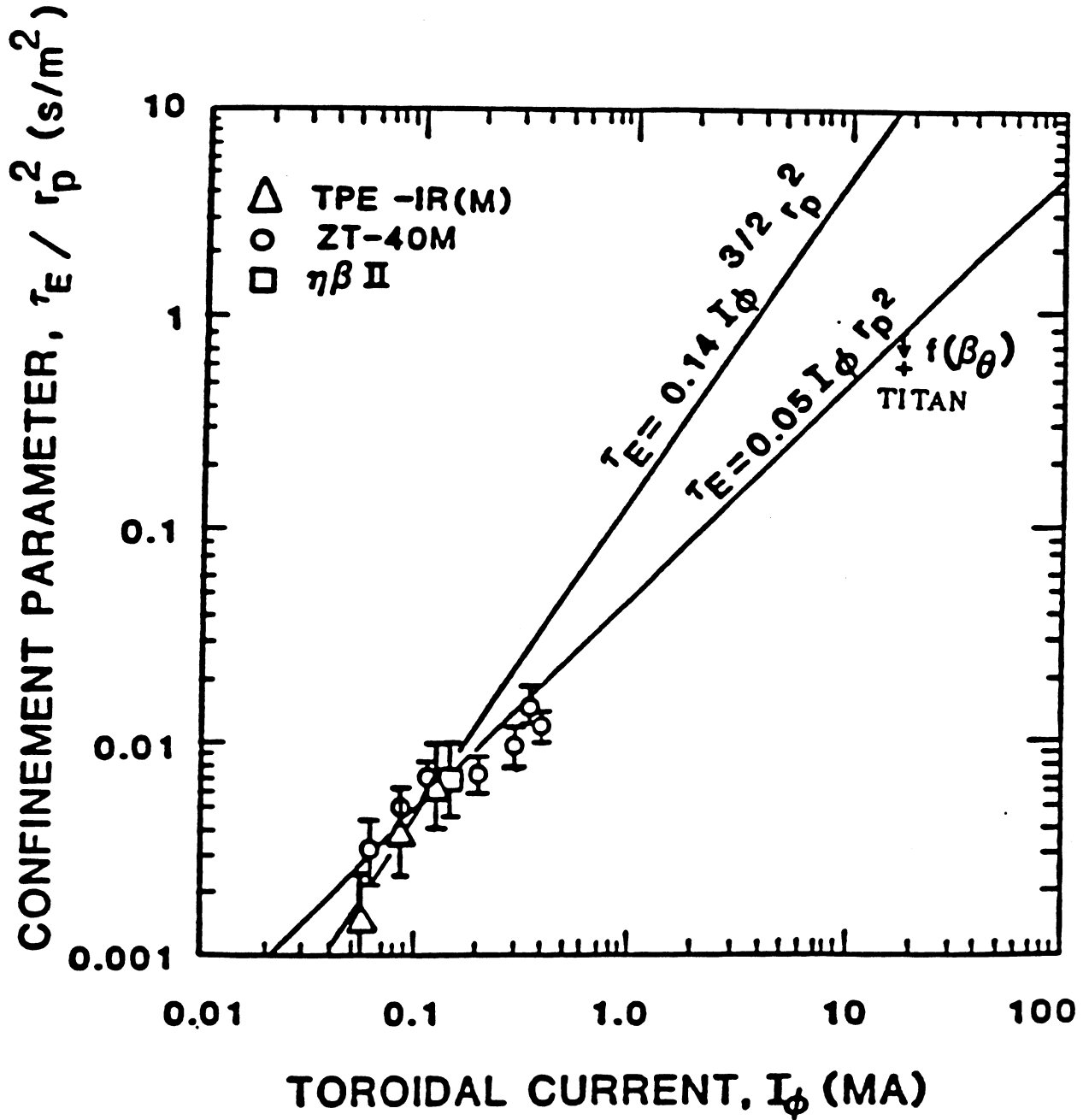


Figure 8.2-4. Variation of the confinement parameter ( $1/\chi_E \propto \tau_E/r_p^2$ ) with plasma current with data from several experiments [20].

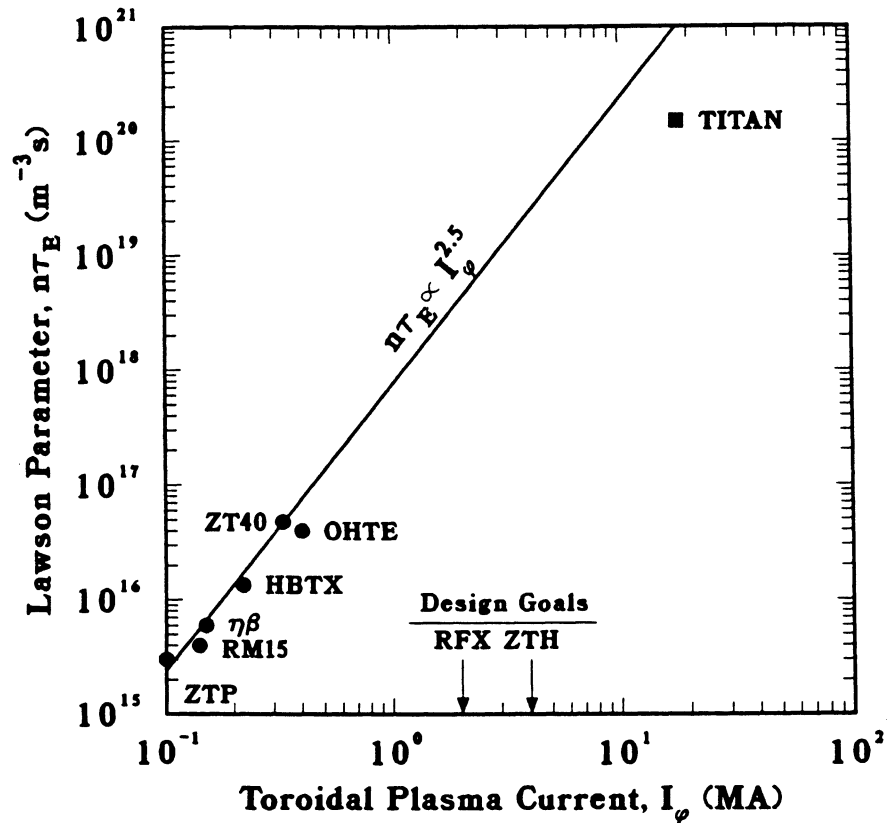


Figure 8.2-5. Variation of the Lawson parameter,  $n\tau_E$ , with the plasma current with data from several experiments [20].

quantities of krypton impurities to the plasma [22]. The radiation loss,  $P_{RAD}$ , increased, the beta remained relatively constant, and the ohmic input power,  $P_{OHM}$ , increased only slightly. The data for the krypton-injection experiment shown on Figure 8.2-6 are in quantitative agreement with this prediction and offer the potential for the beta-limited RFP to radiate (more-or-less uniformly) a large fraction of its energy without significantly reducing the global energy confinement time.

This potential for highly radiative plasmas is important for the compact, high-MPD reactor embodiment in order to control and distribute the expected high heat fluxes uniformly over the first wall. Generally, the highly radiative plasma regime without degrading overall confinement is not available to the tokamak plasma; radiation loss is added to intrinsic losses and degrades the overall confinement.

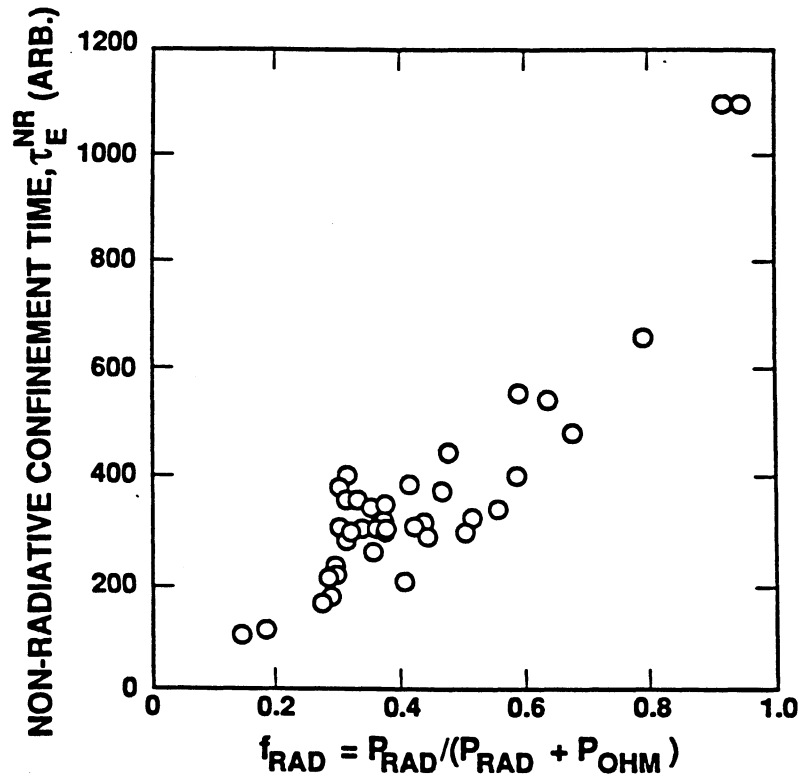


Figure 8.2-6. Scaling of the non-radiative energy confinement time with the fractional radiative power loss in the ZT-40M experiment [22].

### 8.2.3. Reactor Implications

The TITAN parametric systems model (Section 3) was used to investigate the impact of the RFP confinement (*e.g.*,  $\beta_\theta$ ,  $\tau_E$ ,  $f_{RAD}^c$ ) on the reactor cost. The COE increases as  $\beta_\theta$  is decreased, as is shown in Figure 8.2-7, which is caused primarily by the need to establish and drive more plasma current, as is reflected in increased OFCD power consumption and increased coil mass (reduced MPD). Values of  $\beta_\theta$  much below  $\sim 0.1$  result in substantial increases in COE.

Using the experimental scaling of the confinement time,  $\tau_{Ee} \propto I_\phi^\nu \tau_p^2 f(\beta_\theta)$ , the impact of the plasma current scaling exponent,  $\nu$ , on achieving the minimum-COE TITAN-I design is illustrated in Figure 8.2-8. For each respective constant  $\nu$  curve, the condition  $\tau_E(\text{ECON}) \leq \tau_E(\text{PHYS}) \equiv 2(1/\tau_{Ee} + 1/\tau_{Ei})^{-1}$  with  $\tau_{Ei} \simeq 4\tau_{Ee}$  is met to the right (*i.e.*, higher  $\tau_p$ ). The accessibility to minimum-COE designs depends on the value of  $\nu$ . In addition, for  $\nu$  values much below  $\sim 0.8$ , the demands on the OH-coil system during the ohmic-heating transient to ignition and burn can be serious. Also, it should be noted

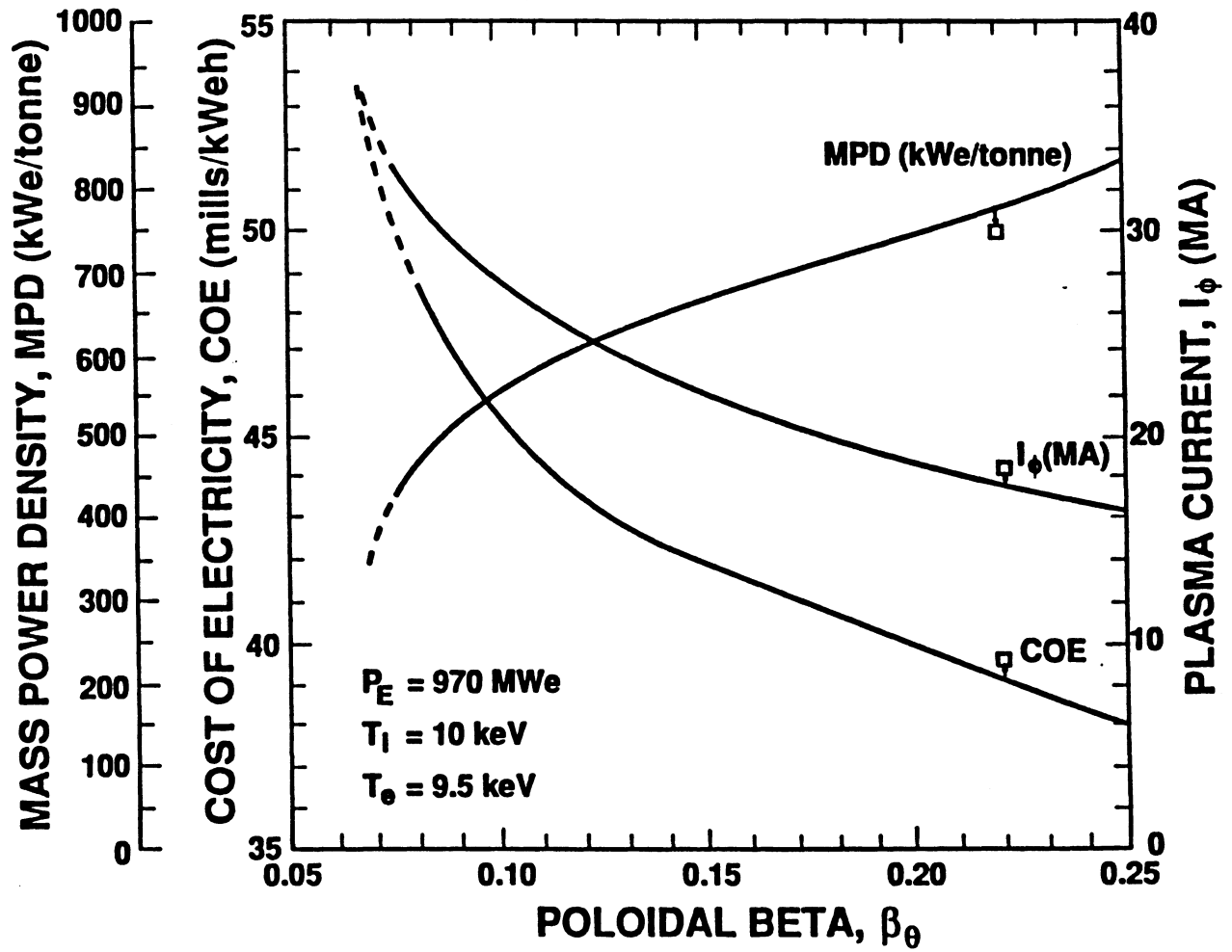


Figure 8.2-7. Dependence of minimum-COE TITAN-I design values on poloidal beta; the near-minimum-COE TITAN-I reference design values are also shown.

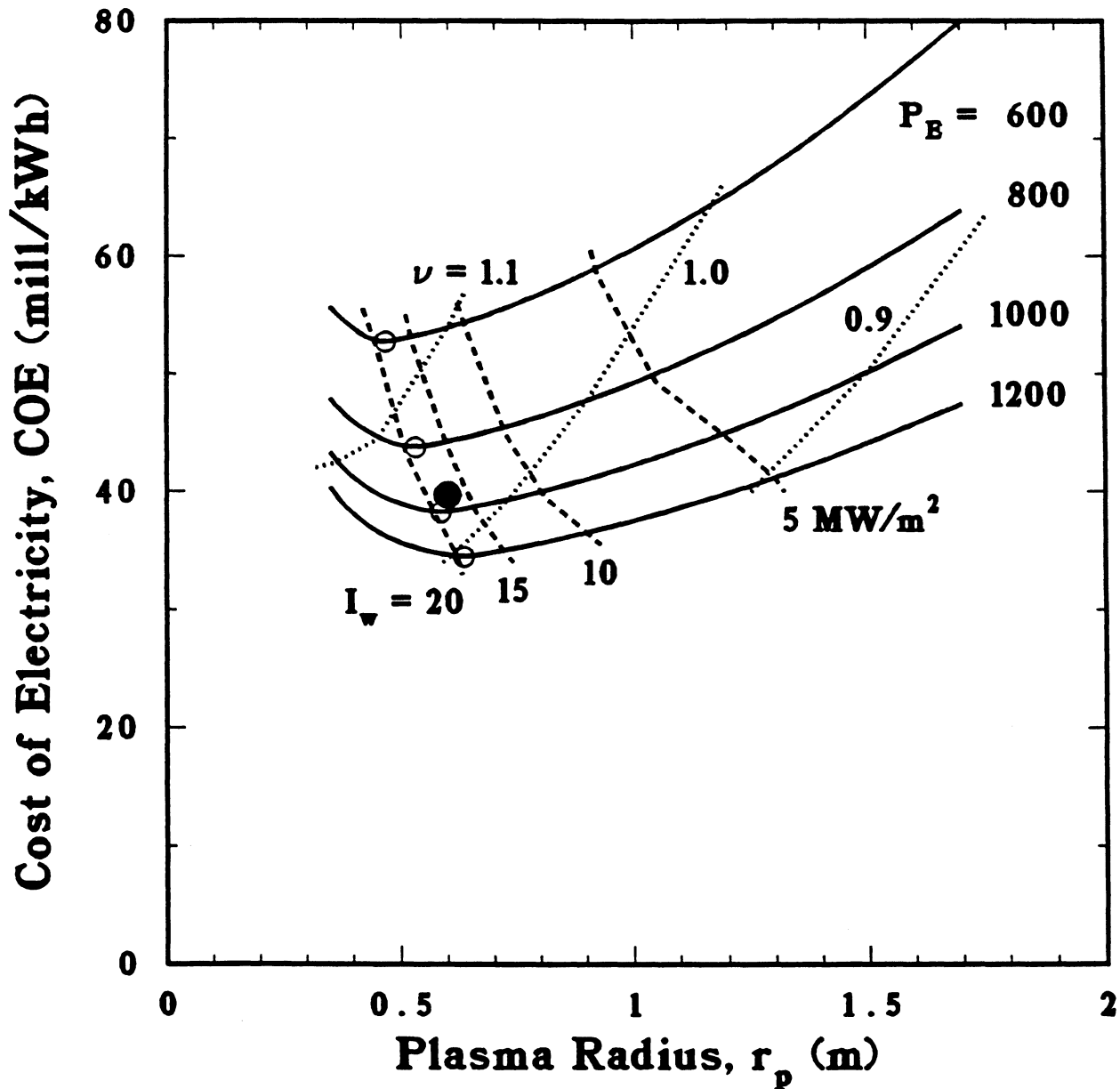


Figure 8.2-8. Parametric trade-off of TITAN-I cost with level of confinement required ( $\tau_{Ee} = C_\nu I_\phi^\nu r_p^2 f(\beta\theta)$ ,  $\tau_{Ei} = 4\tau_{Ee}$ ), expressed as the magnitude of exponent  $\nu$  required for  $\tau_E(\text{ECON}) \leq \tau_E(\text{PHYS}) = 2(1/\tau_{Ei} + 1/\tau_{Ee})^{-1}$ . Accessible design points are to the right of curves of constant  $\nu$ . Minimum-COE design points with  $\tau_E(\text{OPT}) = \tau_E(\text{ECON})$  for fixed net power output  $P_E$  are indicated by open circles. The near-minimum-COE TITAN-I reference design at  $P_E = 970$  MWe and  $I_w = 18.1$  MW/m<sup>2</sup> is denoted by a filled circle.

that the flexibility of operation of TITAN reactors at lower than nominal power (for load following or checkout) requires better intrinsic plasma confinement (*i.e.*, higher  $\nu$ ).

It should be re-emphasized that the scaling given on Figures 8.2-2 and 8.2-3, although reproducible and representative of a statistically large number of discharges, does not occur for all machine conditions. Operating conditions have been observed where  $T_e(0)$  scales less than linearly with plasma current, and the product  $n_e T_e(0)$  scales less strongly than the square of the plasma current (*i.e.*, beta under certain conditions appear to decrease somewhat with increasing current). These operating conditions may result from inadequate control of  $I_\phi/N$  (*e.g.*, pump out) and field errors, leading to increased  $Z_{eff}$  (a parameter not yet measured experimentally in RFPs), cooling of electrons and heating of ions caused by current-driven instabilities, changing edge-plasma conditions and plasma profiles, and other unresolved effects. Hence, a range of plasma current exponents in the scaling of  $T_e(0)$ ,  $n_e$ ,  $T_e(0)n_e$ , and  $\beta_\theta$  exists, ultimately leading to the range of  $\tau_E$  (PHYS) scalings suggested in Figure 8.2-4 as  $\nu$  is varied. Better control of experimental discharges carried out over a wider range of quasi-stationary, flat-top-current conditions is needed and represents a main goal of the generation of RFP experiments presently under construction [16].

### 8.3. CURRENT DRIVE

At full plasma current of 18 MW/m<sup>2</sup>, the energy stored in the reference TITAN plasma includes  $W_M \sim 5$  GJ of magnetic energy and 0.1 GJ of kinetic energy. The magnetic stored energies internal to the plasma are 0.3 GJ in the toroidal field and 0.4 GJ in the poloidal field. The magnetic energies outside of the plasma are < 2 MJ in the toroidal field and 4 GJ in the poloidal field for zero OH-coils current (6 GJ for OH-coils in full forward-bias current). Since, the toroidal magnetic stored energy internal to the plasma is supplied by the poloidal-field circuit during the start-up, the reference TITAN design requires a poloidal flux of  $L_p I_\phi \simeq 250$  Wb to achieve full plasma current. Because of the large plasma resistance in the TITAN designs, an inductively pulsed burn would be sustained for a pulse length of the order of  $L_p/R_p \simeq 200$  to 400 s. Therefore, steady-state operation is essential considering issues such as the total power balance, thermal cyclic fatigue in a high-power-density environment, as well as the costs of on-site energy storage (frequent grid-assisted start-up seems unlikely) and thermal storage. An inductively pulsed RFP reactor is a possibility [23]. The parameters of such a reactor, however, should be optimized to minimize the plasma resistance, which results in larger plasmas, lower power density, and possibly the use of superconducting coils throughout the FPC.

### 8.3.1. Reactor Conditions

A number of current-drive options for the RFP have been considered (Section 8.2). For the TITAN reactors, helicity injection by the oscillating-field current drive (OFCD) has been selected as the mean to sustain the toroidal plasma current.

The major parameters of TITAN-I OFCD system are presented in Table 8.3-I. Although oscillations in the plasma current and toroidal flux are small ( $\delta I_\phi/I_\phi = 0.02$  and  $\delta\phi/\phi_o = 0.035$ ), the reactive power flow across the plasma surface and at the OFCD power supply terminals can be large, requiring careful and possibly expensive energy management. Figure 8.3-1 gives the variation of the main power flows for the TITAN-I OFCD system which uses the main confining magnets for the OFCD.

A circuit model was developed that simulates the major elements associated with OFCD in order to determine the injected and/or dissipated powers (Section 7). The model was used to quantify the need for toroidal and poloidal gaps or insulating breaks in structures such as the first wall, which will have currents induced by the OFCD. It is concluded that these breaks are needed to achieve acceptable current-drive efficiencies ( $\sim 0.35$  A/W). Detailed analysis of the TITAN-I and TITAN-II designs revealed a preference for the following: (1) series winding of all OFCD coils; (2) the positioning of these coils as close to the plasma as possible; and (3) in the case of coil sets with small amplitude oscillations about large average currents, the splitting of the coil set into a set devoted to the oscillation and another set to produce the mean current. Future work should focus on effects of field errors introduced by gaps during current oscillations, a better modeling of helicity balance and profile changes, and the generation of a better engineering understanding of the interaction of the OFCD system with other major FPC subsystems (*e.g.* equilibrium control, impurity control, and startup and shutdown systems).

### 8.3.2. Physics Data Base

Tests of OFCD on the relatively resistive ZT-40M experiment proved encouraging but inconclusive [24]. The key experimental parameters, as for the reactor study, are the frequency, the  $F$ - $\Theta$  oscillation point, and the phase angle between poloidal and toroidal drive voltages ( $\pi/2$  at the plasma surface giving theoretically the strongest OFCD effect under ideal conditions). Tests of OFCD on ZT-40M examined modulations of 180 to 200-kA discharges (40 MVA) and 60 to 70-kA discharges (7 MVA). The latter lower power tests were pursued in an effort to minimize modulation-driven plasma/wall interactions.

Table 8.3-I.  
COMPARISON OF OFCD IN TITAN DESIGNS

	TITAN-I	TITAN-II
Average plasma current, $I_\phi$ (MA)	17.82	17.82
Drive frequency, $f$ (Hz)	25.	25.
Toroidal-flux swing, $\delta\phi/\phi_o$	0.035	0.035
$\Theta$ variation	1.499 – 1.616	1.499 – 1.616
$F$ variation	-0.032 – -0.173	-0.032 – -0.173
Toroidal (poloidal) circuit power (MW):		
Plasma Poynting power, $P_P^*$	3959.99 (247.31)	3959.99 (247.31)
Plasma dissipation, $P_\Omega$	28.55 ( 0. )	28.55 ( 0. )
First-wall dissipation, $P_{FW}$	0.00 ( 0.01)	0.00 ( 0.01)
Blanket dissipation, $P_B$	1.04 ( 0. )	0.01 ( 0.17)
Terminal reactive power, $P_i^*$ (MW):		
TF coils	503.88	1413.77
OH coils	74.92	101.99
EF coils	~ 0.	~ 0.
Trim coils	113.44	147.16
Coil dissipation, $P_H$ (MW):		
TF coils	47.38	11.44
OH coils	0.13	0.17
EF coils	~ 0.	~ 0.
Trim coils	1.95	2.49
Real (lost) terminal power, $P_T$ (MW):		
TF coils	74.00	38.23
OH coils	1.62	1.15
EF coils	~ 0.	~ 0.
Trim coils	3.44	3.46
TF-coil DC power, $P_{H,\theta}^{SS}$ (MW)	29.15	9.34
Power-supply dissipation, $P_{PS}$ (MW) <sup>(a)</sup>	6.92	15.34
Total dissipation, $P_D$ (MW)	85.93	58.19
Current-drive power, $P_{CD}$ (MW)	56.83	48.85
Efficiency, $I_\phi/P_{CD}$ (A/W) <sup>(b)</sup>	0.33	0.36

(a) Assuming the power supplies are 99% efficient ( $Q_{PS} = 100$ ).

(b) Based on total power consumed including driver efficiency and transmission losses.

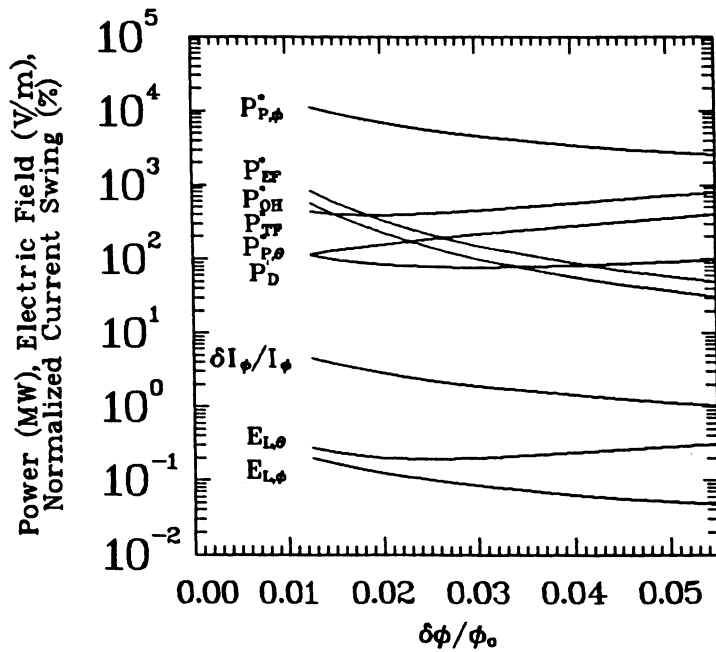
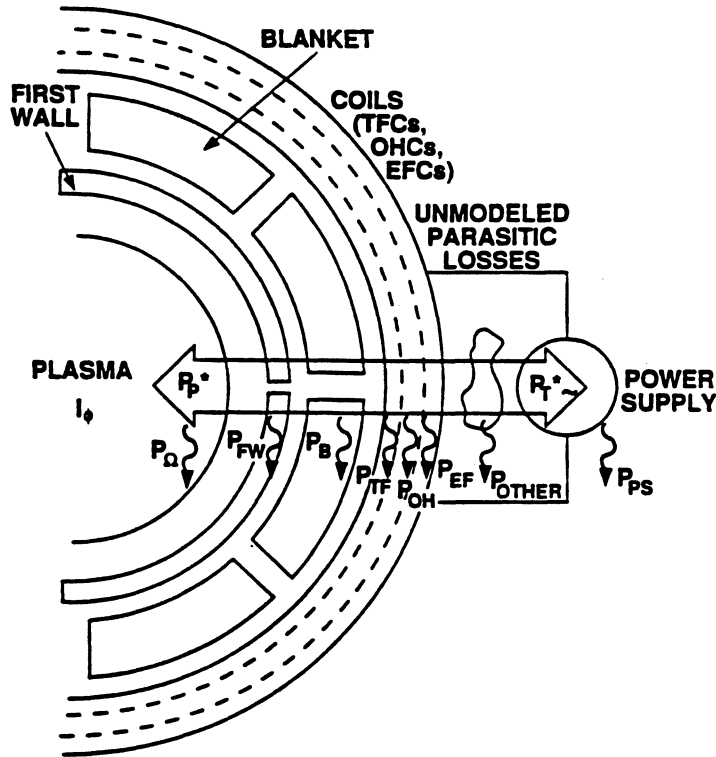


Figure 8.3-1. Variation of the main power flows, current swings, and driver voltages as a function of toroidal flux swing for the TITAN-I OFCD system.

Figure 8.3-2 gives the time dependence of plasma current, reversed toroidal field ( $B_{\phi R}$ ), average toroidal field (flux), and reactive powers on the ZT-40M experiments for (1) no drive, (2) drive (phase shift of  $\pi/2$ ), and (3) anti-drive (phase shift of  $-\pi/2$ ). As predicted by theory,  $I_{\phi}$  is reduced in the anti-drive mode, but failure to drive significant current in the drive mode possibly resulted from modulation-driven plasma-wall interactions. Attempts to drive current in lower-current discharges requiring less modulation of a colder, higher-resistance plasma also proved inconclusive. In addition to agreeing with theoretical predictions of the impact of the modulation phase, measured spatial and temporal behavior of the mean toroidal field within the plasma during modulations also agree with OFCD theory. Future tests of the OFCD principle must await high-temperature, lower-resistance plasmas that require less modulation of  $F-\Theta$ , lower frequency, reduced plasma-wall interaction, and ideally use an RFP with a fixed separatrix in order to better control the equilibrium and the plasma/wall interaction.

### 8.3.3. Reactor Implications

Steady-state operation of the high-power-density TITAN-I reactor is mandatory, and some form of current drive will be required. The TITAN plasma is seeded with impurities and is highly radiative in order to spread the heat load uniformly over the first wall and to reduce the divertor-plate heat load to manageable levels. Seeding of the plasma with impurities, however, increases the current-drive requirements through increased  $Z_{eff}$  and plasma current dissipation. Attempts to reduce the plasma ohmic loss and rate of helicity injection through OFCD by increasing the plasma temperature also requires higher impurity concentrations and  $Z_{eff}$  to maintain the design value of  $f_{RAD}$ . It was found that the TITAN OFCD requirements under this  $f_{RAD}$  constraint actually increased as the average plasma temperature was increased above the 10-keV design value.

Assuming that the large ( $\sim 4$  GW) Poynting flux to and from the plasma under the OFCD conditions can be efficiently managed and the field errors introduced by gaps in the FPC components during OFCD oscillations can be controlled, the management of 500 to 1,500-MW reactive powers at the TF-coil terminals with high- $Q$  efficiency (Table 8.3-I) at reasonable cost (10-15\$/kVA) represents the main engineering concern. The impact of the circuit  $Q$ -value on COE and other reactor parameters is illustrated in Figure 8.3-3. It can be seen that  $Q$ -values much below  $\sim 50$  will begin to have economic impact on the TITAN-I design.

Plasma parameters, particularly the  $F-\Theta$  oscillating point, will also have serious cost and design impacts. Deeper reversals (*i.e.*, more negative  $F$ -value) are desirable since

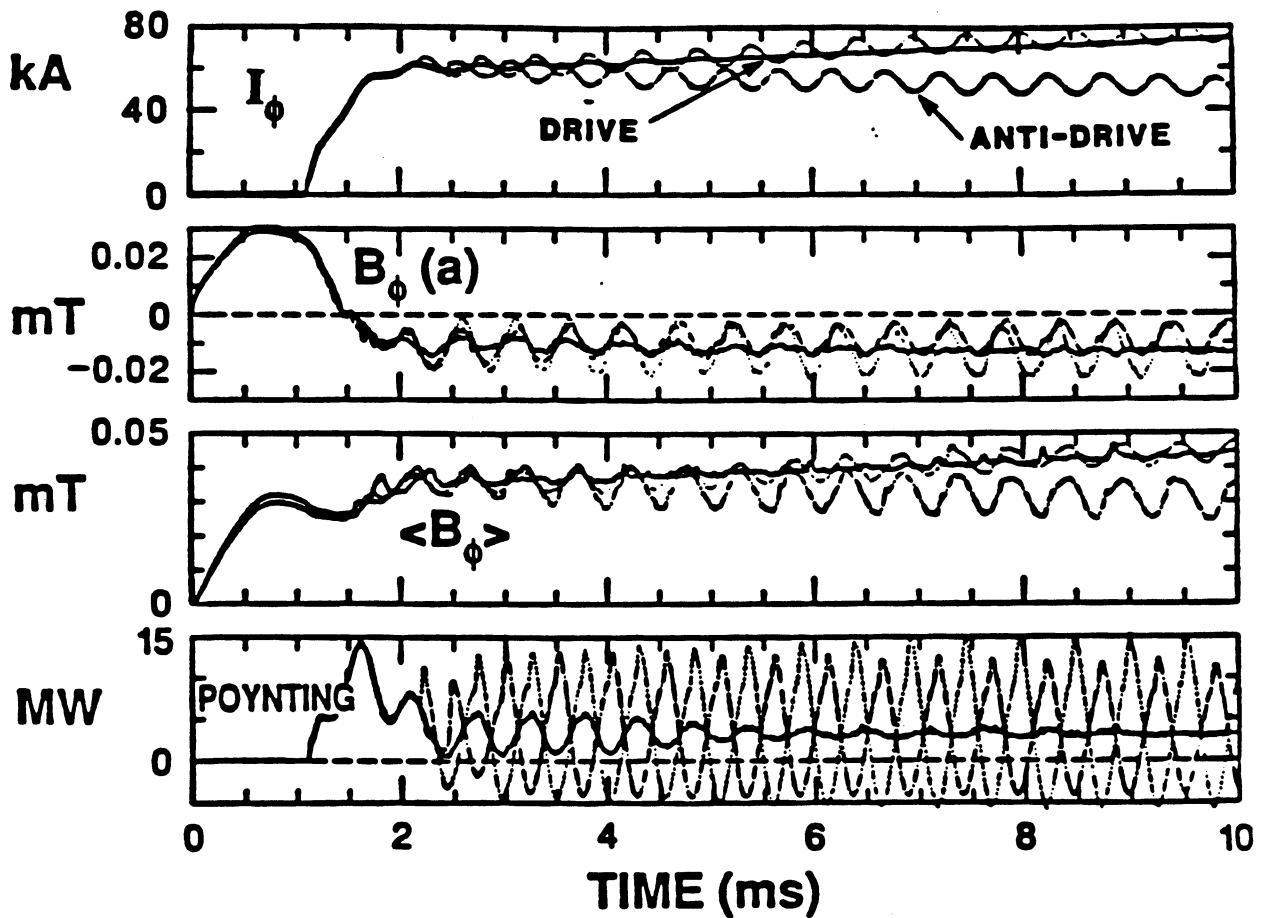


Figure 8.3-2. Low-power OFCD discharge results from Reference [24]. Shown are traces of current, edge toroidal field, toroidal flux, and Poynting vector for a standard discharge, a discharge with the optimal phase between toroidal and poloidal OFCD circuits for driving current, and a discharge with the optimal phase in the OFCD circuit for anti-drive.

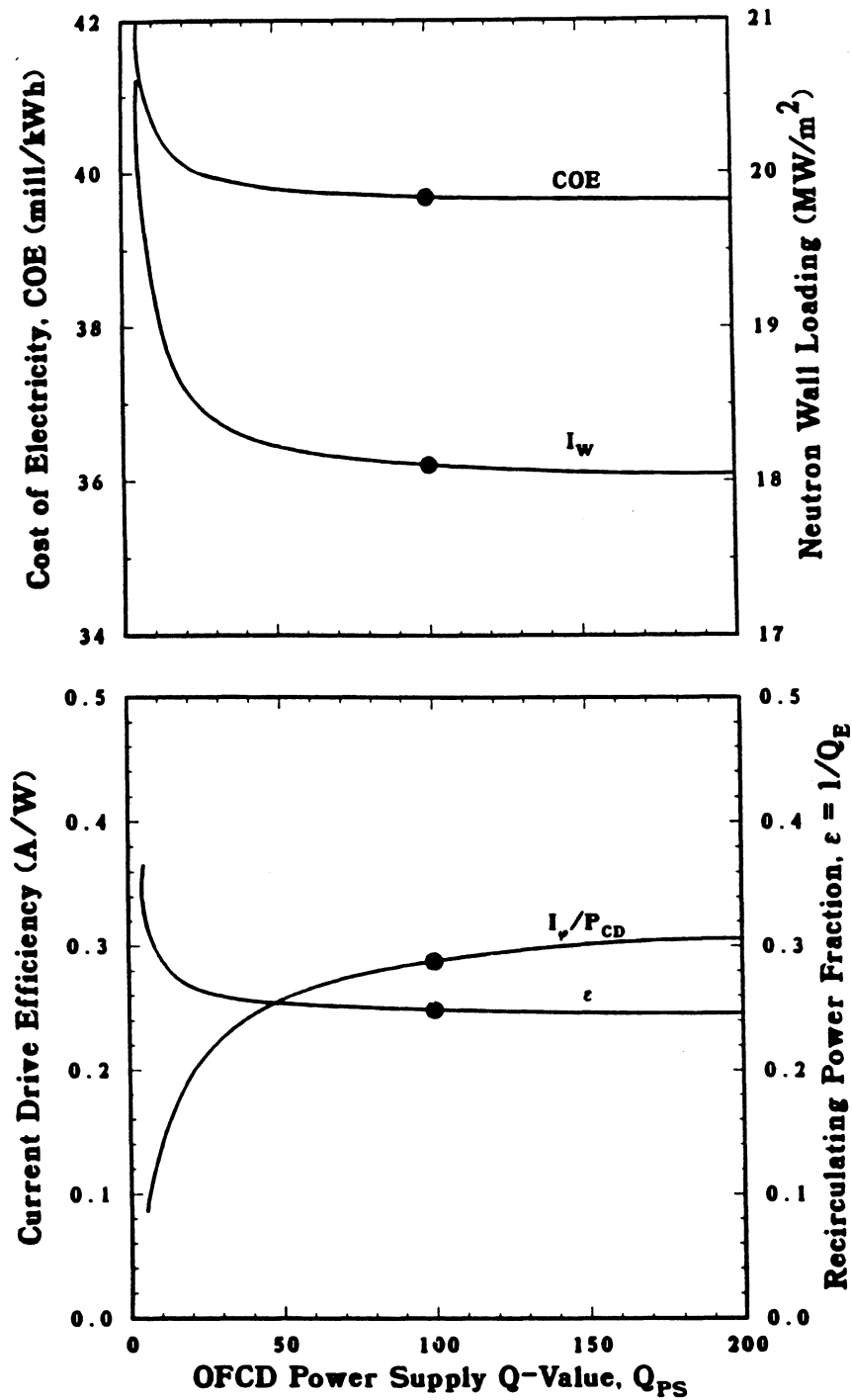


Figure 8.3-3. Impact of OFCD power supply Q-value on TITAN-I operating parameters. The TITAN-I reference case is denoted by a filled circle at  $Q_{PS} = 100$ .

the design reported in Table 8.3-I oscillates close to loss of reversal. Deeper reversals, however, will increase an already large TF-coil circuit reactive power, as well as increasing steady-state losses in the TF and divertor coils. Figure 8.3-4 illustrates the impact of the  $F$ - $\Theta$  operating point on the overall TITAN-I design point.

Lastly, the impact of OFCD frequency and modulation amplitude on the plasma resistance and overall confinement represents areas of future concern. Other means to deliver magnet helicity to RFPs also warrant future examination (*e.g.*, DC helicity injection perhaps using the divertor plates as electrodes [25] or RF-driven poloidal current in the lower-density edge plasma).

## 8.4. IMPURITY CONTROL

The design of in-vessel components (divertor plate, limiter, first wall) is a critical issue for all fusion reactors. The key problem is to remove the steady-state plasma power (alpha-particle and ohmic) while maintaining acceptable heat fluxes and erosion rates on all components. In the scoping phase of the TITAN study [1], a simulation of the edge plasma without impurity radiation indicated plasma temperatures in the range of 50 to 100 eV at the first wall and very high heat fluxes on the divertor target. As a result the TITAN reactors operate with a highly radiative plasma with balanced radiation from core, edge, and divertor plasmas. The plasma is deliberately doped with a trace amount of high- $Z$  xenon impurities to create strong radiative cooling and spreading the heat load uniformly over the largest possible area (first wall). This high-radiation regime of operation, which appears to be an essential ingredient for a high-power-density reactor, may be more easily achieved in RFPs than in tokamaks because experimental evidence suggests that RFPs operate with a soft- $\beta$  limit (Section 8.3).

### 8.4.1. Reactor Conditions

The use of either poloidal pump limiters or magnetic divertors in the context of a high-power-density RFP requires that the majority of the plasma self-heating power be radiated uniformly to the first wall and other in-vessel components. Further analysis of the array of 24 poloidal limiter blades suggested in early studies [5] indicated possible problems with gross erosion of those surfaces in contact with the hot edge plasma. The TITAN designs, therefore, are based on toroidal-field divertors to minimize the perturbation to the global magnetic configuration (toroidal field is the minority field in RFPs) and to minimize the coil currents and magnetic forces [26].

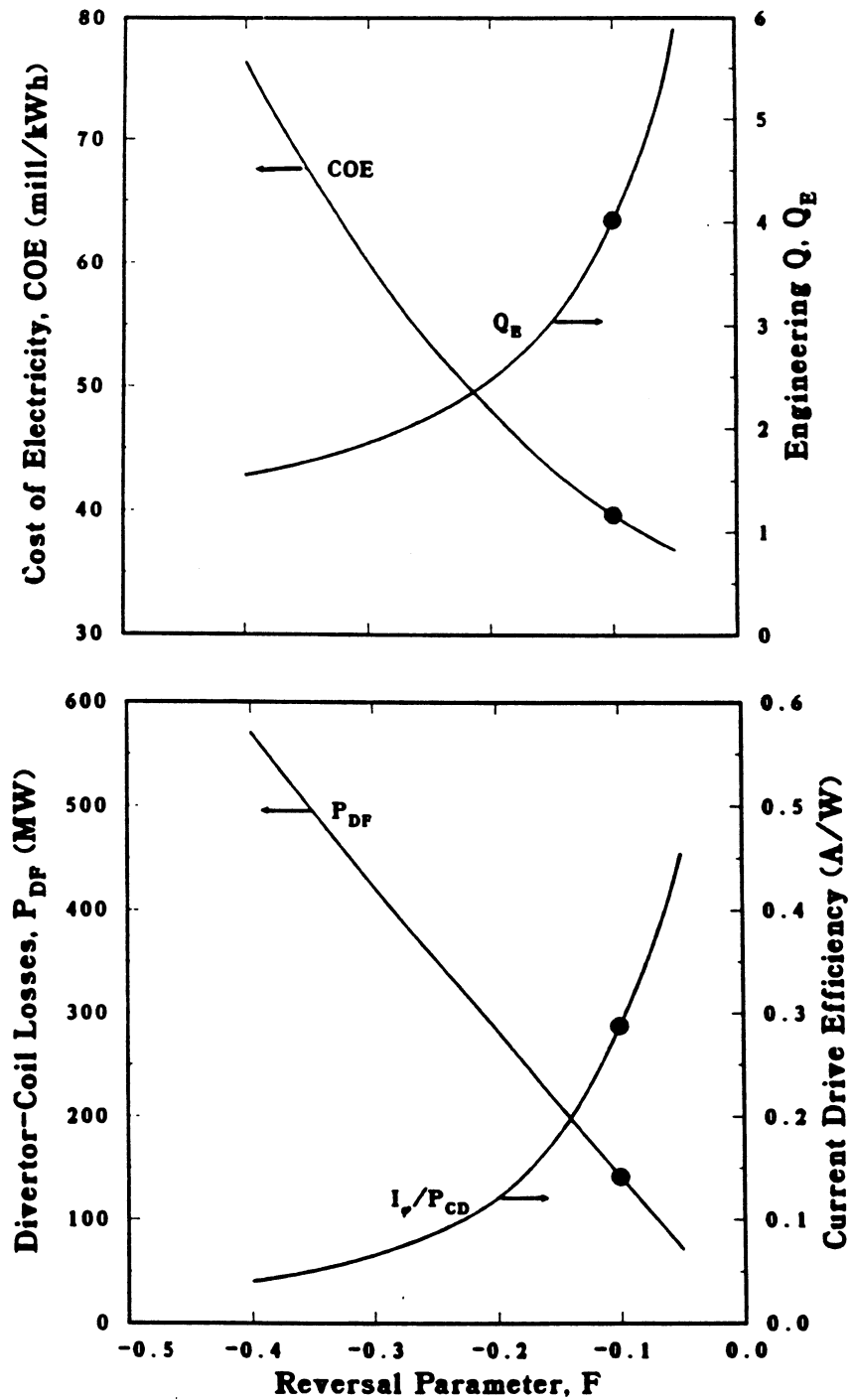


Figure 8.3-4. Impact of the reversal parameter on the overall TITAN-I design and cost. The TITAN-I reference design at  $F = -0.1$  is denoted by a filled circle.

The final TITAN divertor designs represent the result of extensive iterations between edge-plasma analysis, magnetic design, thermal-hydraulic and structural analyses, and neutronics. The TITAN divertors uses an “open” configuration, in which the divertor target is located close to the null point and faces the plasma, rather than in a separate chamber (Figure 8.4-1). This positioning takes advantage of the increased flux expansion in this region which tends to reduce the heat loading on the divertor plate. The high plasma density in front of the divertor plate ensures that the neutral particles emitted from the surface have a short mean free path and only a negligible fraction of these neutral particles enter the plasma (Section 5.5).

The final magnetic design includes three divertor modules, located 120° apart in toroidal direction. The local field ripple produced by these poloidally symmetric toroidal-field divertors amounts to  $\Delta B_R/B_\theta = 0.01-0.02$  with a connection length in the range 70 to 75 m, flux expansion factors in the range 2 to 4, and scrape-off-layer thicknesses of  $\sim 60$  mm. Table 8.4-I compares the impact of the divertor-induced ripple on the magnetic-island width,  $\Delta r$ , with the case where divertors are not used. The magnetic-island widths is estimated from

$$\frac{\Delta r}{r_r} = \left[ 16 \frac{\Delta B_R/B_\theta}{N r_r (dq/dr)} \right]^{1/2}, \quad (8.4-1)$$

where the poloidal field at the plasma surface is  $B_\theta = 5.9$  T, the shear at the reversal surface is  $r_r(dq/dr)_{r_r} = -0.165$ , and the mode number  $N = 2\pi R_T/l_{TF}$ , with  $R_T = 3.9$  m being the major radius and  $l_{TF}$  being the toroidal extent of the toroidal-field perturbation.

The radial profile of edge-plasma density and temperature, as predicted by the edge-plasma transport code ODESSA [27], is given in Figure 8.4-2. The resultant heat flux on the divertor target from an integrated thermal-hydraulics/divertor-plate positioning code (Section 11) are shown in Figure 8.4-3. For the estimated density and temperature profiles in the scrape-off layer, sputter-erosion rates at the first-wall and divertor-plate surface are estimated to be below 0.1 mm/y. These low erosion rates for the high-power-density RFP are possible because of the high-density (low-temperature) first-wall and divertor-plate conditions.

#### 8.4.2. Physics Data Base

Experience operating RFPs with a magnetic separatrix is nonexistent. Although plans exist for shell-less RFP operation with an octapole-like (poloidal-field) separatrix [16,28], this configuration is not relevant to the configuration proposed for the TITAN-I.

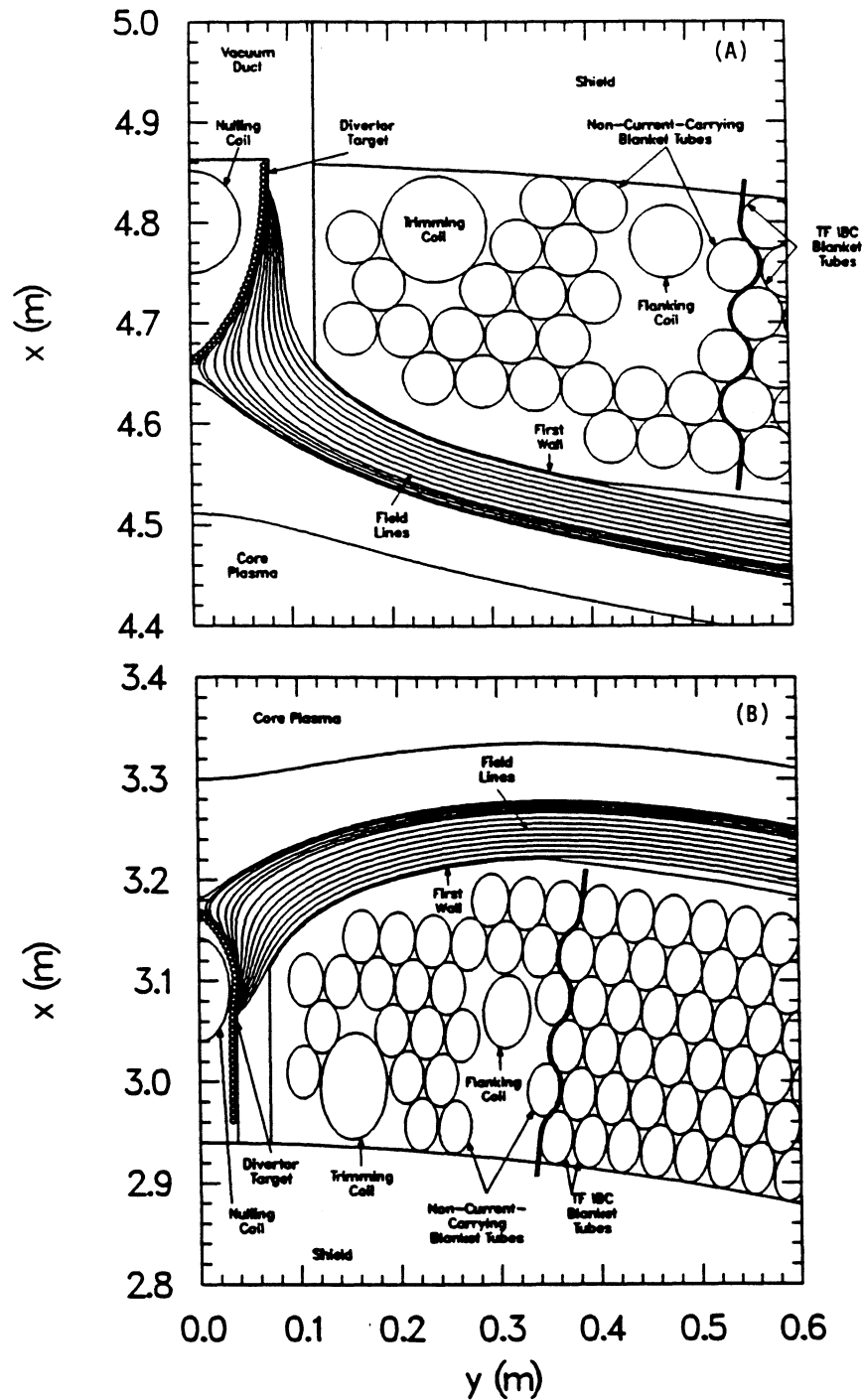


Figure 8.4-1. Outboard (A) and inboard (B) equatorial-plane views of the divertor region for TITAN-I.

Table 8.4-I.

**COMPARISON OF FIELD RIPPLE  
WITH AND WITHOUT TOROIDAL-FIELD DIVERTORS**

	With Divertors		Without Divertors <sup>(a)</sup>
Location	$r_r = 0.55$ m	$r_p = 0.60$ m	$r_p = 0.60$ m
Radial field, $\Delta B_R$ (mT) <sup>(b)</sup>	84/76	136/103	$\sim 10^{-3}$ (2/14)
Ripple parameter, $\Delta B_R/B_\theta$ <sup>(b)</sup>	0.014/0.013	0.023/0.017	$\sim 0$ ( $\sim 0/0.002$ )
Effective mode number, $N$	$> 300$	$> 300$	$\sim 1,000$ (30)
Magnetic-island width, $\Delta r/r_r$	$\leq 0.067/0.065$	$\leq 0.086/0.074$	$\sim 0$ ( $\sim 0/0.025$ )

(a) Values for TITAN-I TF-IBC coils.

Values for TITAN-II copper TF coils are given in parenthesis.

(b) Maximum values at inboard/outboard locations.

### 8.4.3. Reactor Implications

The high-recycling toroidal-field divertor appears to provide the most viable impurity-control scheme for the high-power-density RFP reactor. Although the local ripple induced by the divertor is large, the size of the associated magnetic islands can be held to a small fraction of the distance between the reversal and plasma (separatrix) surfaces. The divertor should be positioned as close as is possible to the plasma in order to minimize local perturbation in the magnetic topology and also to minimize coil dissipation.

The impact of the distance between the divertor coils and the plasma on the power consumption by the divertor coils is shown in Figure 8.4-4 for the TITAN-I, wherein added shielding could conceivably be required if the insulator radiation lifetimes fall below the estimated design values (Section 10.2). The distance plotted on Figure 8.4-4 is defined by the toroidal-field null and the nulling-coil inner surface. These results were obtained by varying the divertor-coil radial location and currents for a fixed current density of  $38 \text{ MA/m}^2$  and a fixed angle of  $3.5^\circ$  between the nulling- and flanking-coil current centers. The lower bound on  $\Delta s/r_p$  in Figure 8.4-4 is set by the maximum

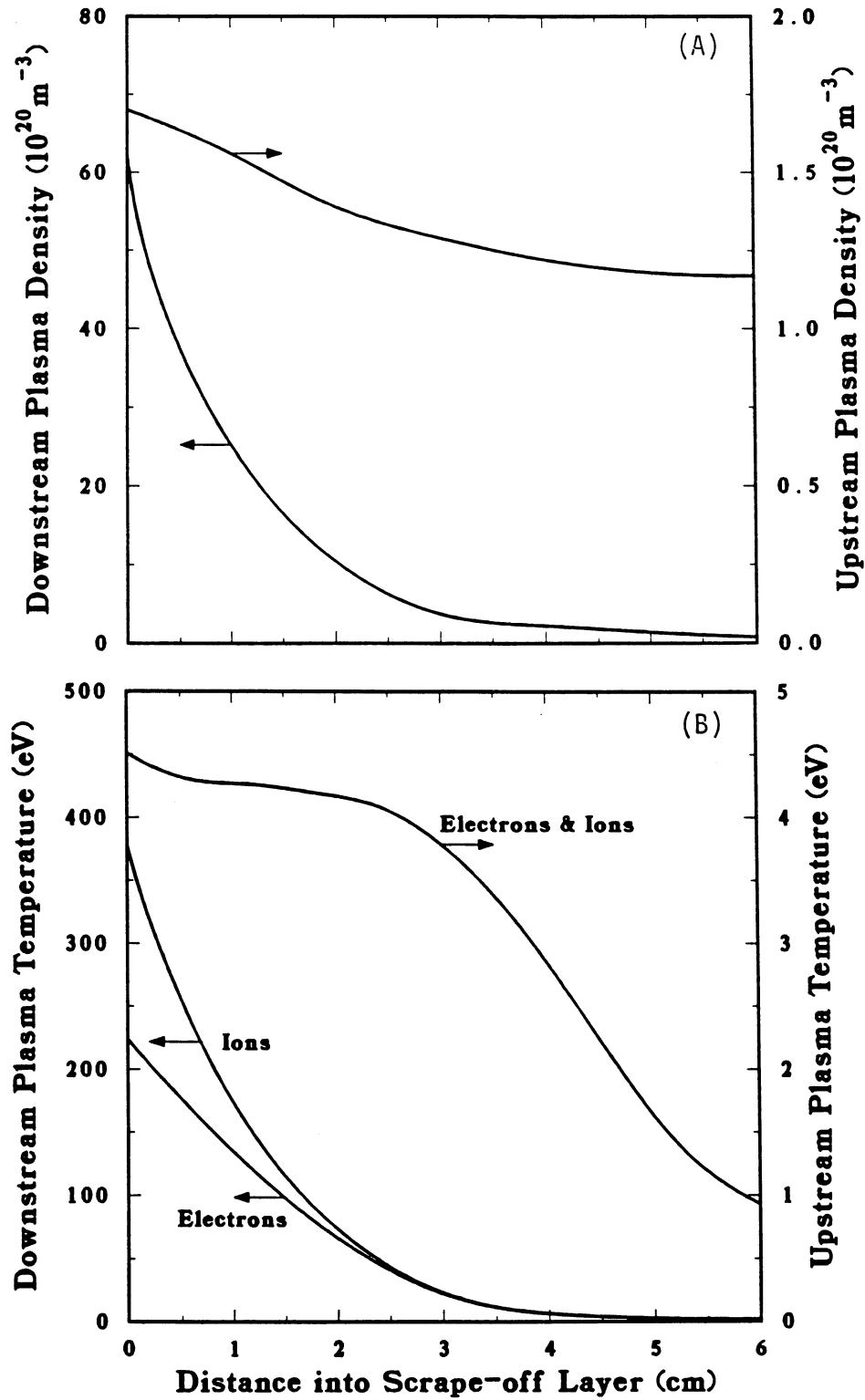


Figure 8.4-2. Radial profile of edge-plasma density (A) and temperature (B) in the scrape-off layer for upstream and downstream axial positions in TITAN-I.

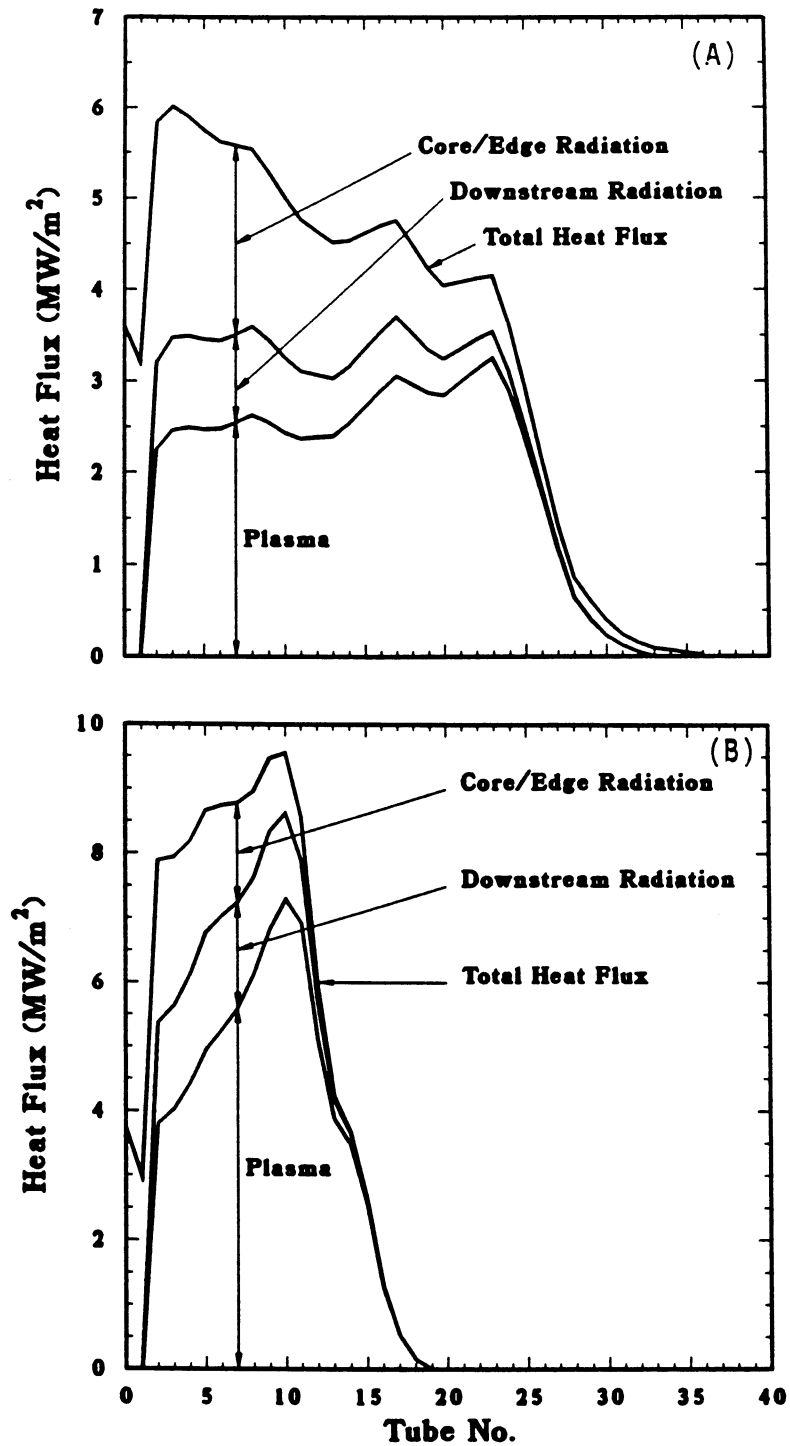


Figure 8.4-3. Heat flux distribution on the outboard (A) and inboard (B) sections of the TITAN-I divertor target. Coolant tubes are numbered from the apex or symmetry point of the target between the nulling coil and the core plasma.

heat flux (*i.e.*, size of divertor-field plume) and is  $\geq 0.07$  and  $\geq 0.12$  for TITAN-I and TITAN-II, respectively. Recirculated power considerations set upper bounds on  $\Delta s/r_p$ .

The operation of the TITAN divertors is very sensitive to precise positioning of the separatrix and the edge-plasma field lines with respect to the divertor target. Control of the divertor-coil current as well as the overall phasing of the divertor operation with the start-up and subsequent OFCD transients present other concerns. Generally, operation of OFCD with a fixed separatrix location and a hot plasma at the separatrix should reduce both the plasma resistance, plasma wall interaction, and hence, the OFCD requirements, provided the scrape-off region does not promote additional helicity dissipation [29].

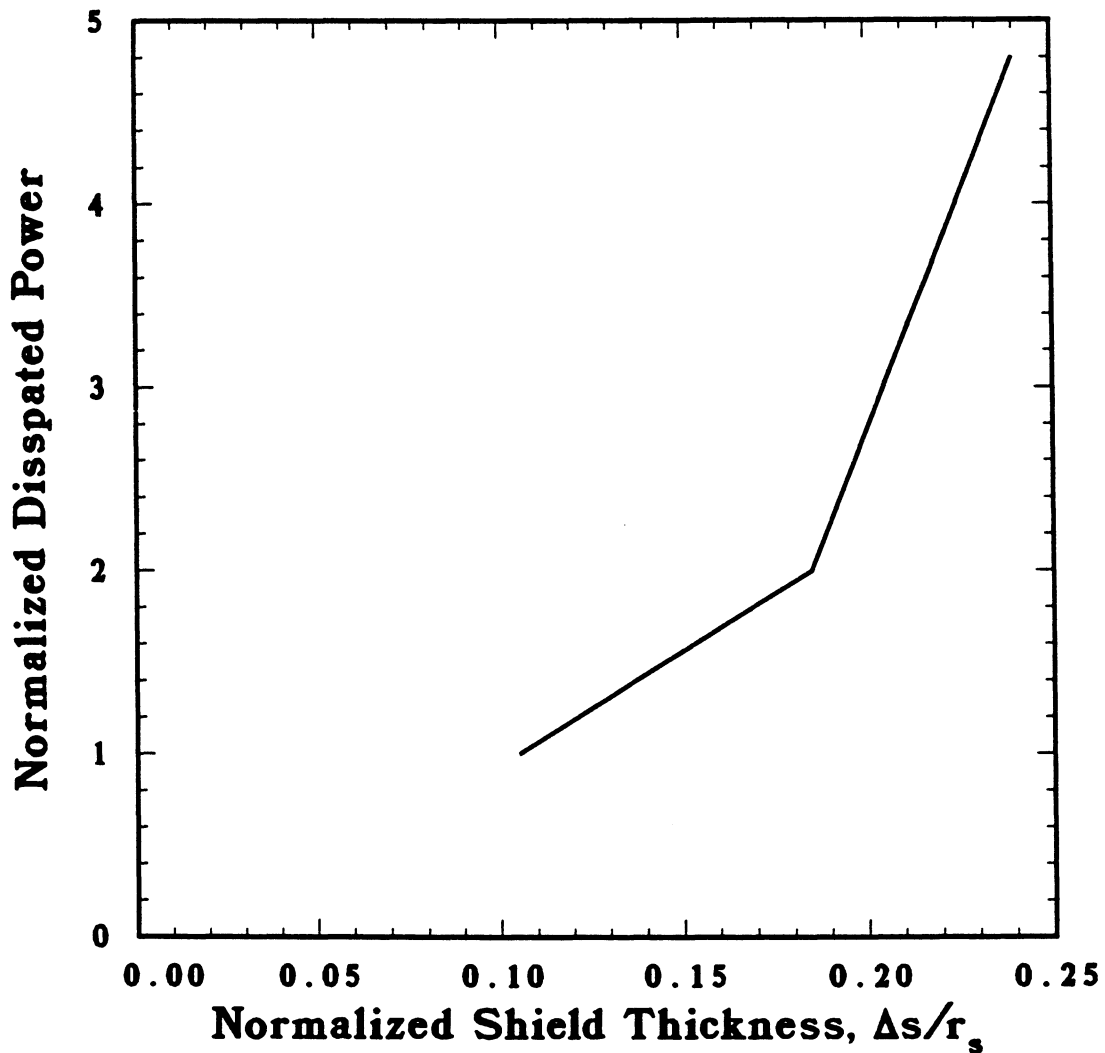


Figure 8.4-4. Sensitivity of TITAN-I divertor-coil power consumption to normalized shield thickness.

## 8.5. FORMATION AND START-UP

### 8.5.1. Reactor Conditions

The four main phases of the TITAN start-up towards achieving ohmic ignition and ultimately a steady-state,  $I_\phi = 18$ -MA burn are illustrated in Figure 8.5-1. The proposed start-up scenario includes: (1) a 1 to 10-ms formation phase (0.1 to 0.2 MA), (2) a fast current ramp (2 to 3 s, 0.1→10 MA), (3) a slow current ramp (8 to 20 s, 10→18 MA), and (4) steady-state burn. Throughout this current ramp-up phase, active equilibrium control (by main equilibrium-field and trim coils) will be required. Impurity control should probably start during the fast current-ramp phase and the separatrix position held fixed during the start-up transients. The OFCD system may start operation during the slow-ramp phase to assist in achieving the full plasma current. Initially, about 0.2 to 0.3 Wb of toroidal flux would be injected by the TF coil. The majority of the  $\sim 5$  Wb of toroidal flux contained within the final burning plasma, however, would be generated through the poloidal-field (PF) coil system by the RFP dynamo and, hence, presents an added, but small, flux requirement for the ohmic-heating (OH) coils.

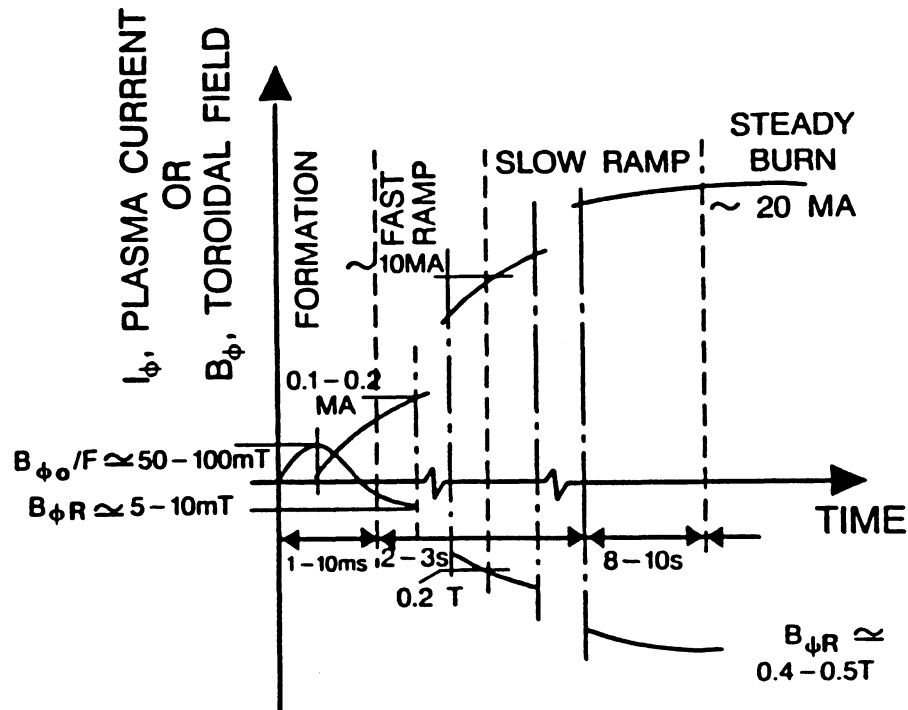


Figure 8.5-1. Schematic of TITAN start-up and burn cycle.

### 8.5.2. Physics Data Base

A body of experimental evidence is beginning to accumulate that better defines the windows for RFP breakdown, formation, and ramp-up. The status in each of these areas is summarized. Because of the present position of the RFP physics program, a majority of the RFP data base pertains to the formation/current ramp and, to a lesser extent, to the confinement areas.

#### 8.5.2.1. Breakdown

Plasma discharge and subsequent RFP formation generally occurs for values of the ratio of toroidal electric field to initial filling pressure,  $E_\phi/P_o$ , that are similar to tokamak values, but closer to electron runaway conditions. For example, for the JET experiment, a value of  $E_\phi/P_o \geq 0.66 \times 10^4$  V/m-torr is reported [30], compared to 1 to  $2 \times 10^4$  V/m-torr for ZT-40M [31], which is close to electron runaway conditions. Figure 8.5-2 gives typical breakdown and formation characteristics for a range of tokamaks and for ZT-40M. Generally, breakdown and discharge formation are not problems for RFPs, but the degree of pre-ionization can greatly influence the discharge quality and poloidal-flux consumption [33,34]. Since, to date, stable and reliable RFP formation appears to require a high  $E_\phi$ , the generally common  $E_\phi/P_o$  values for both RFPs and tokamaks give significantly higher values of  $P_o$  required to create a robust RFP. An initial electric field of  $E_\phi = 55$  V/m is indicated in Figure 8.5-3 for matched-mode operation.

A toroidal-field line of strength,  $B_{\phi o}$ , in the presence of a vertical field,  $B_V$ , will intersect the first wall and thereby prevent the formation of a continuous discharge if the ratio  $B_V/B_{\phi o}$  is too large. The condition for the confinement of a single toroidal trajectory with a field null at a minor radial position,  $r_o$ , is given by

$$\frac{B_V}{B_{\phi o}} \leq \frac{\epsilon}{2\pi} \sqrt{1 - (r_o/r_p)^2}, \quad (8.5-1)$$

where  $\epsilon = r_p/R_T$  is the inverse plasma aspect ratio. For TITAN with  $1/\epsilon \simeq 6.3$  and setting  $r_o \simeq 0.5 r_p$  result in  $B_V/B_{\phi o} \leq 0.02$ .

In addition, a drift constraint,  $E_\phi/(B_V/B_{\phi o}) \geq 10^3$  V/m, has been suggested for JET [32]. This drift constraint together with Equation 8.5-1 results in  $E_\phi \geq 22$  V/m, which is about a factor of 2 below experimental values derived from the ZT-40M experience. Therefore, breakdown voltage in the range 500 to 1,000 V may be required for the reactor. Careful designs that minimize field errors can possibly reduce these start-up voltages.

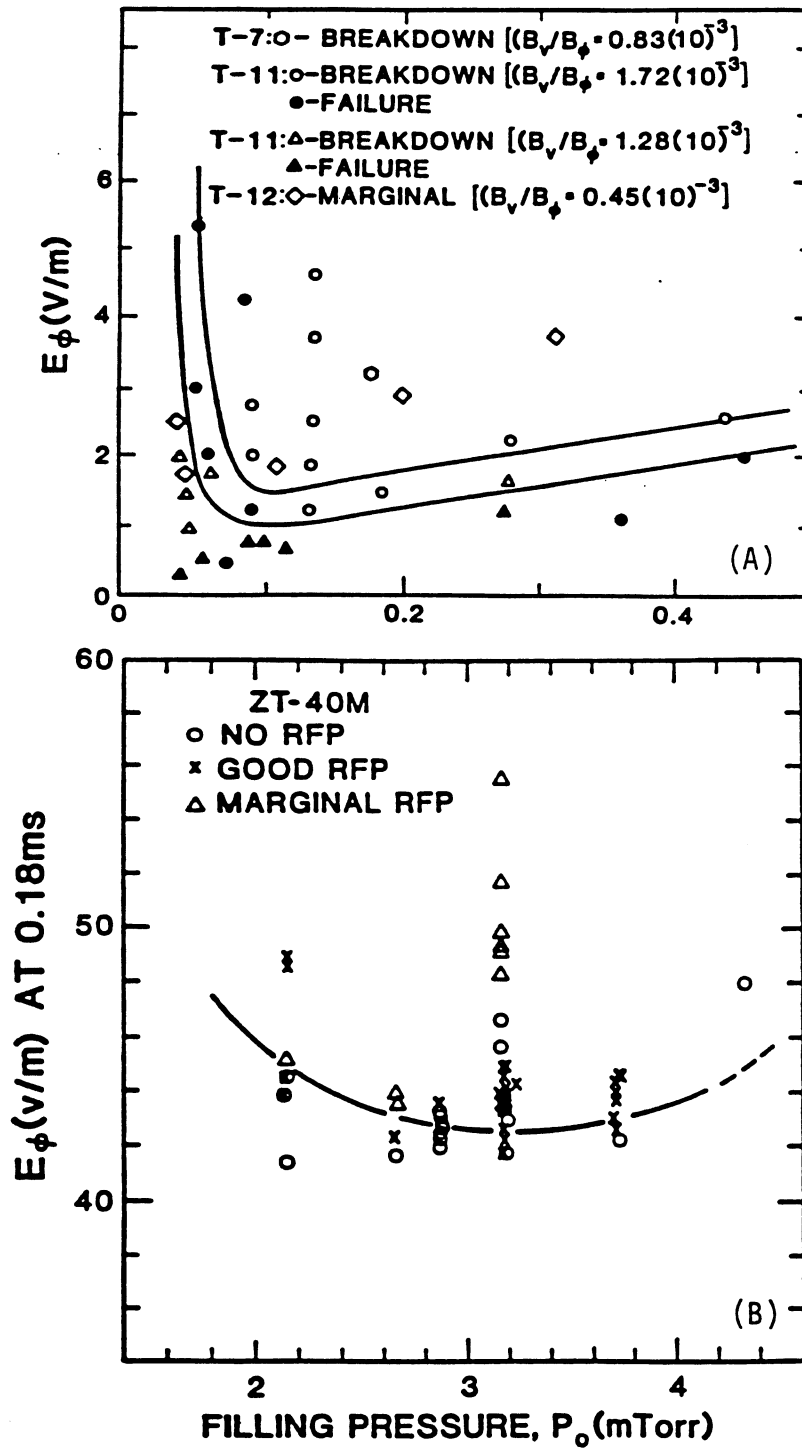


Figure 8.5-2. Typical breakdown curves for (A) tokamak [32] and (B) RFP formation [33,34].

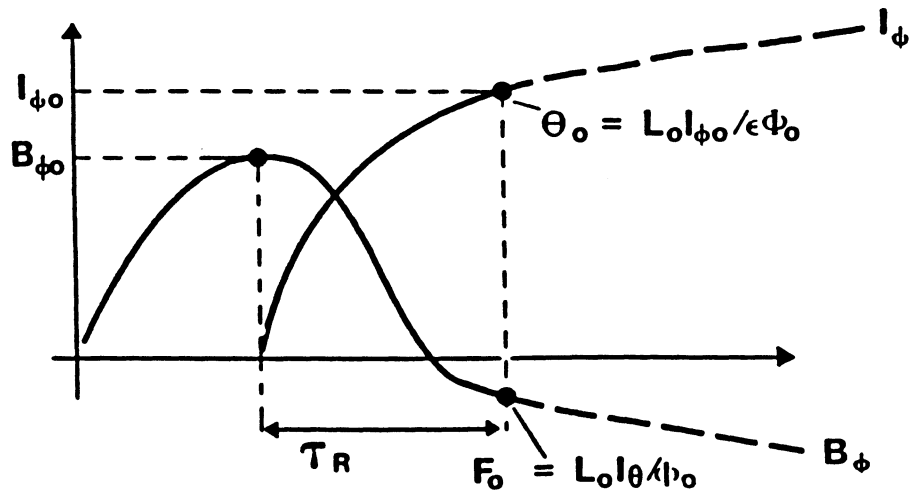
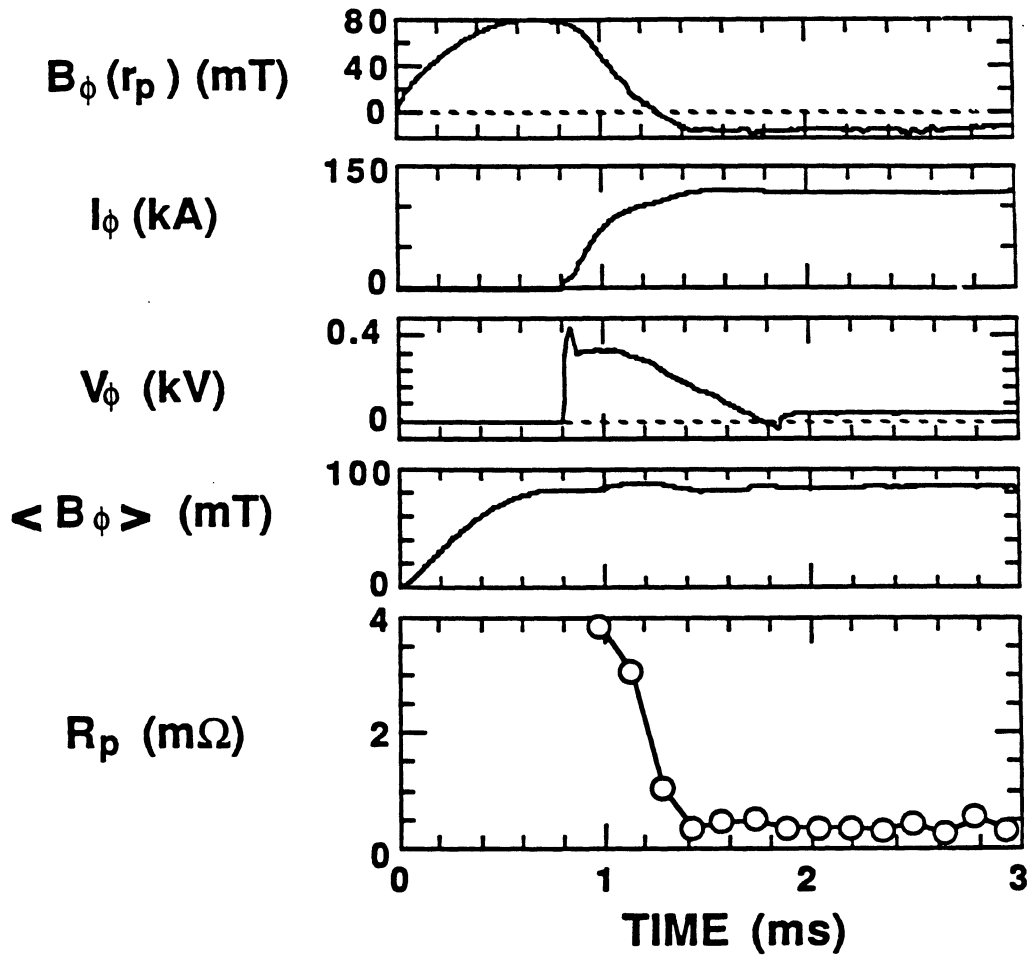


Figure 8.5-3. Typical matched-mode RFP formation for ZT-40M leading to the values of  $\Theta_0$ ,  $F_0$ , and  $I_{\phi 0}$  [35] used as initial conditions for start-up, ignition, and burn simulations.

### 8.5.2.2. RFP formation

In order to establish the parameters of the “seed” RFP, the relationship between  $B_{\phi o}$  and the average toroidal flux within the initial RFP,  $\langle B_{\phi} \rangle$ , must be determined (Figure 8.5-3). Generally,  $\langle B_{\phi} \rangle \simeq B_{\phi o}$  for RFP formation. Figure 8.5-4 shows the relationship between  $B_{\phi o}$  and  $\langle B_{\phi} \rangle$  for a range of ZT-40M discharges, illustrating the experimental basis for this assumption. For a given  $\langle B_{\phi} \rangle$  and the initial pinch parameter,  $\Theta_o$ , the initial (minimum) RFP current or current density is determined from

$$I_{\phi o} = 5r_p \Theta_o \langle B_{\phi} \rangle. \quad (8.5-2)$$

Hence, for  $\langle B_{\phi} \rangle \simeq B_{\phi o} = 0.05$  T at formation, and TITAN plasma conditions of  $\Theta_o \simeq 1.5$  and  $r_p = 0.6$  m, the initial RFP current is  $I_{\phi o} \simeq 0.2$  MA.

Although the specification of  $\Theta_o$  and  $\langle B_{\phi} \rangle$  at formation determines an initial current density (*e.g.*,  $j_{\phi o} \simeq 0.2$  MA/m<sup>2</sup> for TITAN), other more dominant constraints may exist. For example, the ZT-40M experiment exhibits a minimum current-density limit which translates empirically to  $j_{\phi o} \geq 0.4$  MA/m<sup>2</sup>, below which RFP formation is difficult. This constraint is not well understood, but the application of such a constraint to TITAN represents a conservative connection to experiment and for the above condition would require a doubling of  $B_{\phi o} \simeq \langle B_{\phi} \rangle$ . Secondly, a number of RFP experiments [6] have shown an impurity burn-through constraint, shown in Figure 8.5-5 for ZT-40M. For these conditions, burn-through requires that  $j_{\phi}/n \geq 10^{-20}$  MA m. This constraint, however, when applied to the 0.2- to 0.4-keV plasmas expected for these formation conditions places the plasma strongly in the electron runaway regime. If the runaway regime is to be avoided, which may or may not be a requirement, higher densities will be required (*e.g.*, for  $\xi \equiv v_D/v_{THE} \leq 0.01$ ,  $n \geq 2 \times 10^{19}$  m<sup>-3</sup> for  $j_{\phi} = 0.4$  MA/m<sup>2</sup> and  $T \simeq 0.2$  keV).

Generally, if the density pump-out is too great prior to toroidal-field reversal for a given initial filling pressure,  $P_o$ , unreliable RFP formation occurs [31], as is shown in Figure 8.5-6(A). Similarly, for a given  $P_o$  a maximum initial bias field,  $B_{\phi o}$ , is found above which RFP formation does not occur [31], as is also shown in Figure 8.5-6(B). Although RFPs form at lower values of  $B_{\phi o}$ , these RFPs have excessive poloidal-flux consumption, as is shown in Figure 8.5-6(B), for the ZT-40M conditions examined. It should be noted that a variable and poorly controlled wall condition creates hysteresis and related unpredictable effects in many of these data correlations. The constraints of Figures 8.5-6(A) and (B) have been combined in Figure 8.5-6(C) to eliminate the filling pressure as a variable and perhaps to reduce the impact of these unresolved wall effects on these data. The result is a relationship between average plasma density and initial

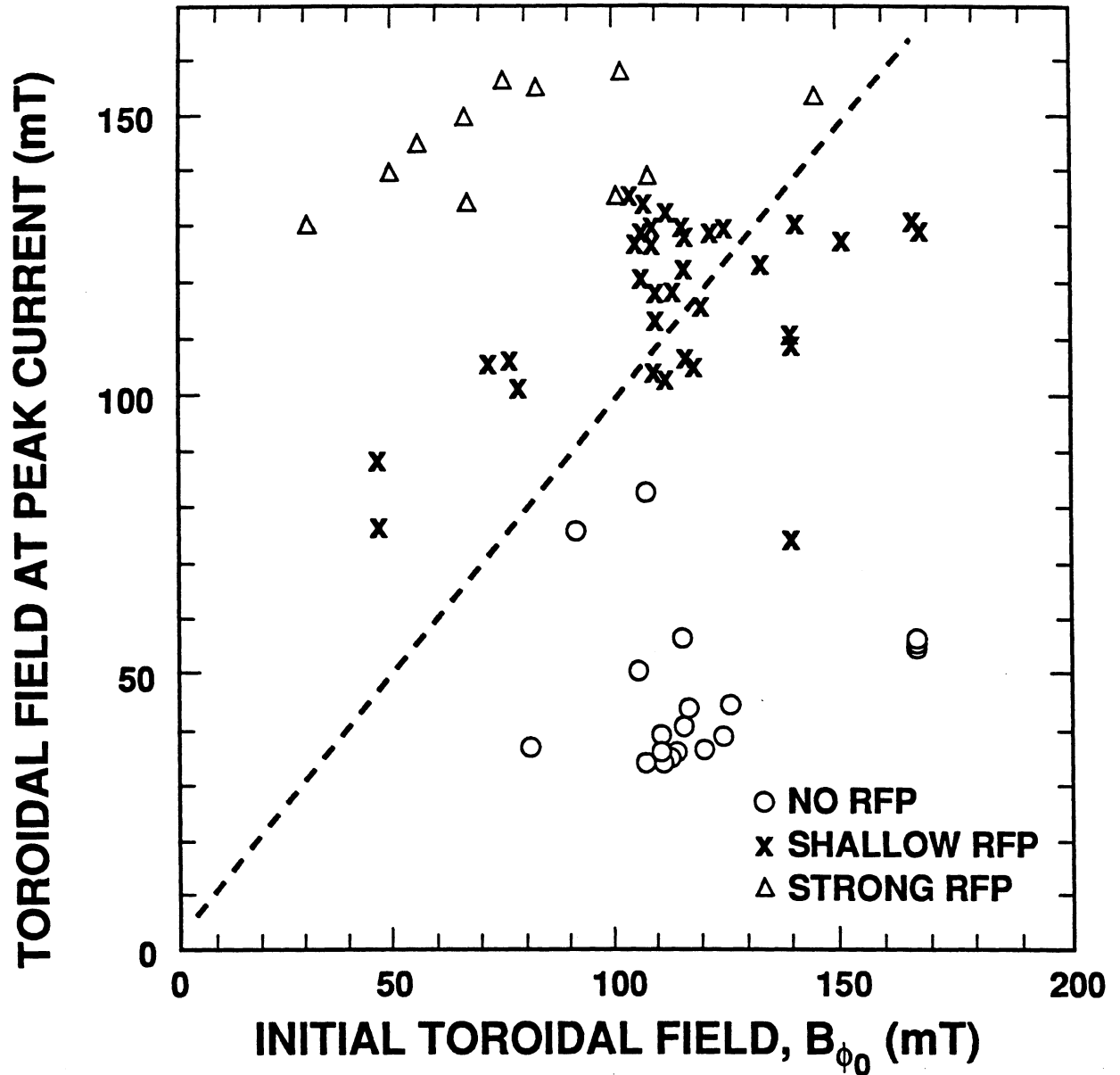


Figure 8.5-4. Relationship between  $B_{\phi_0}$  and  $\langle B_{\phi} \rangle$  for a range of ZT-40M discharges [31, 34] where robust RFP formation occurred, as well as no RFP formation and/or very shallow, spheromak-like RFPs were formed.

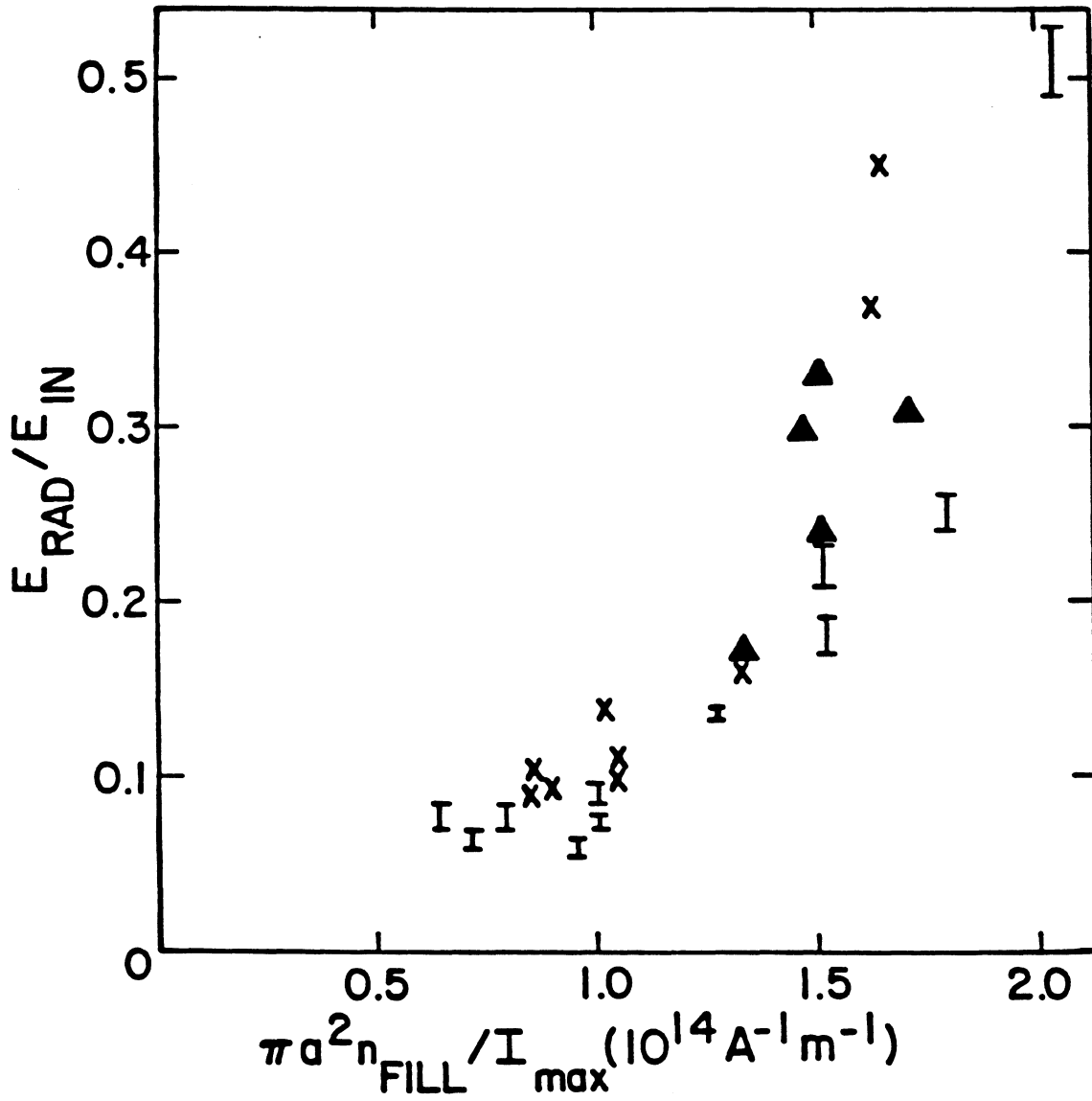


Figure 8.5-5. Typical impurity burn-through constraint for ZT-40M [31].

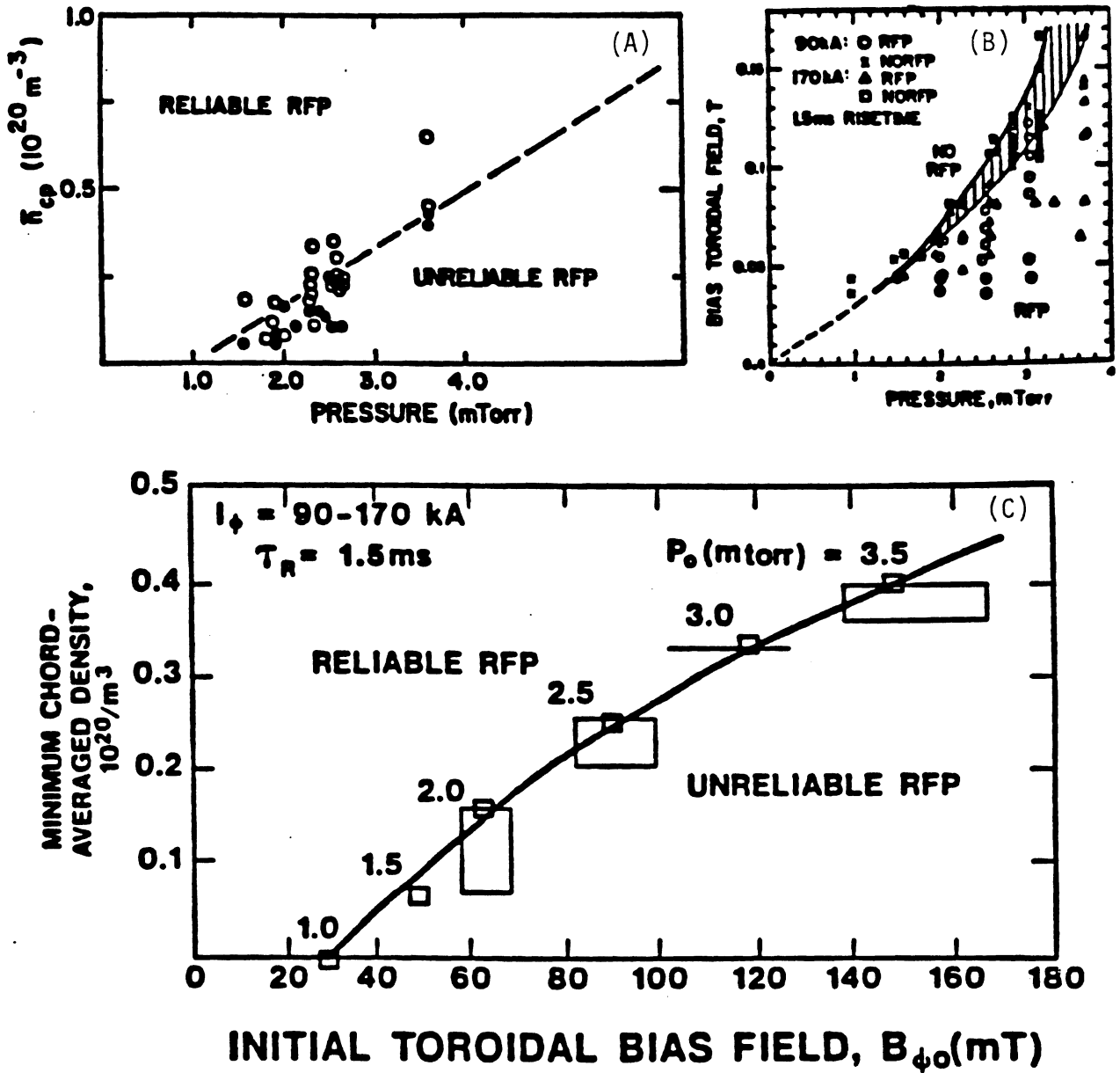


Figure 8.5-6. Typical RFP formation windows showing: (A) dependence on a critical plasma density, (B) magnitude of the initial toroidal bias field, and (C) a combination of the two constraints [31].

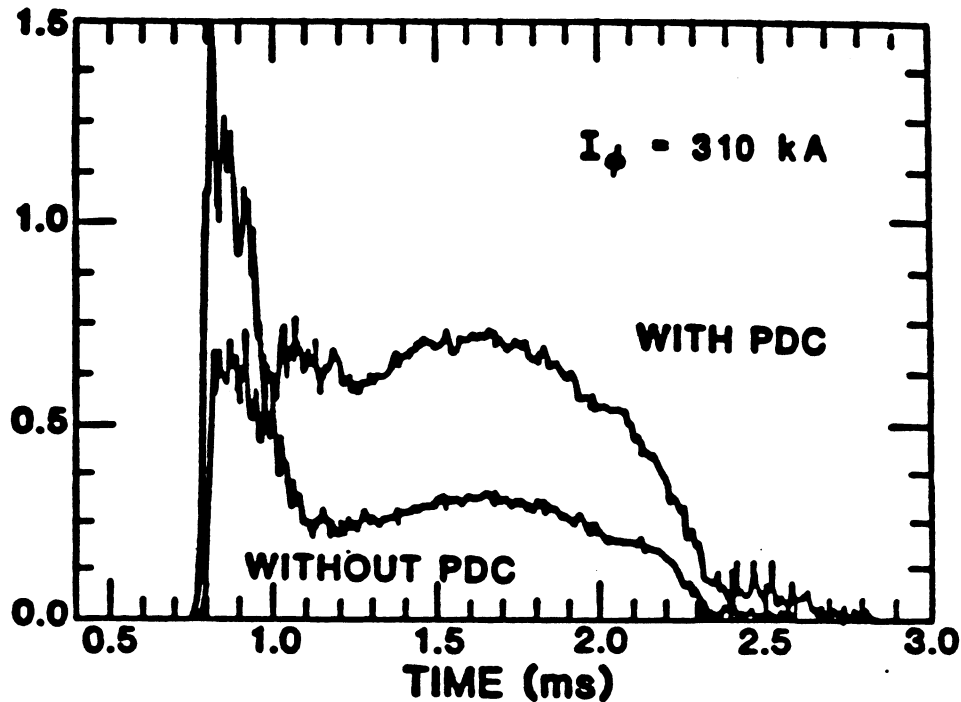


Figure 8.5-7. Loss of density or pump-out for a typical ZT-40M discharge. Also shown is the impact of pellet fueling on reducing pump-out [36].

bias field that may be useful in assuring robust RFP formation. Typically, for values of  $B_{\phi 0}$  being considered, the minimum critical density for reliable RFP formation is above that needed to assure a reasonable safety margin against electron runaway upon RFP formation.

Most present-day RFPs experience a significant loss of density or pump-out upon formation, as is shown in Figure 8.5-7. The degree of density reduction between the initial filling pressure and the final RFP formation is not well understood but it depends strongly on wall preconditioning. Hence, the pump-out is expressed in terms of the ratio of initial filling density,  $n_o$ , to the final RFP plasma density,  $n > n_c$ , and the assumption must be made for the reactor that pump-out and  $P_o$  can be minimized, thereby minimizing the  $E_{\phi}$  required under start-up conditions.

### 8.5.2.3. Current ramp-up

While the formation phase leading to the low-current ( $\sim 0.2$ -MA) “seed” RFP is characterized by a rapid current rise (150 MA/s for the case shown in Figure 8.5-3),

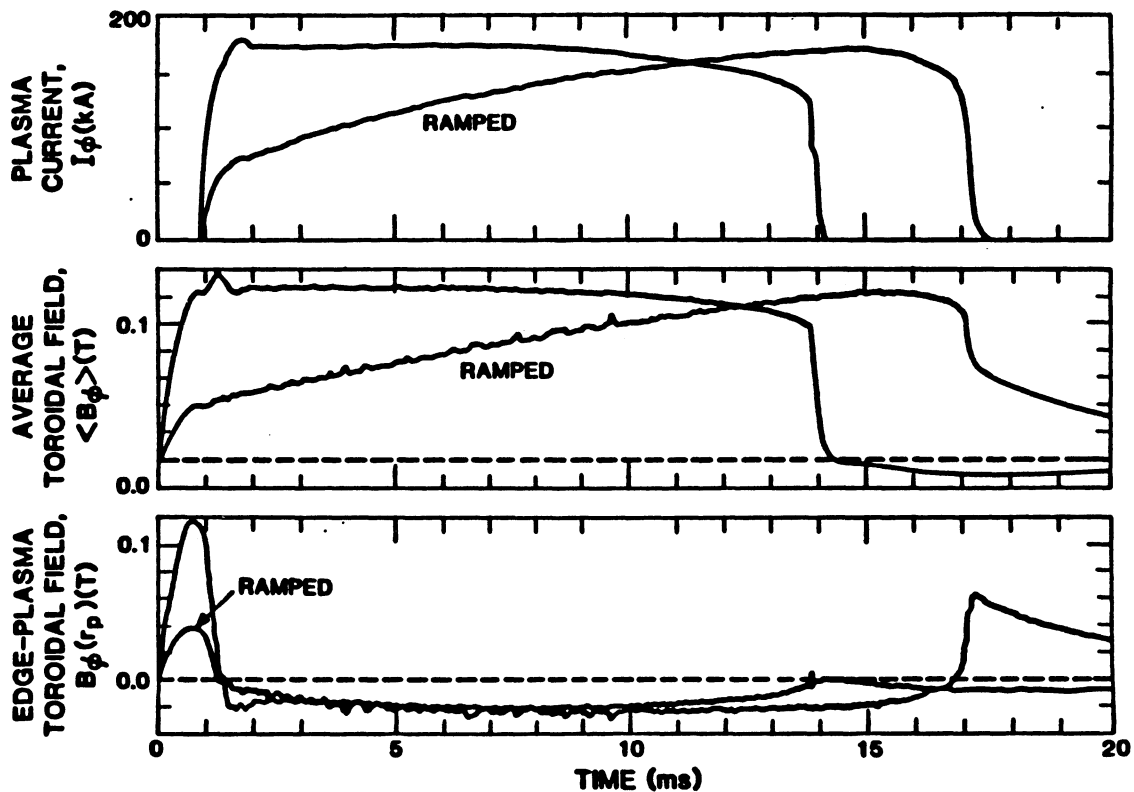


Figure 8.5-8. Slow and fast current ramps in ZT-40M [31].

and the flux consumption can be a small fraction of the inductive flux delivered to the plasma, the subsequent current ramp to ohmic ignition and burn ( $I_\phi = 18$  MA) represents a greater concern from the viewpoint of resistive flux consumption and the implication on OH-coil and related power-supply designs. Figure 8.5-8 shows that slow current ramp rates (9 MA/s) have been achieved in ZT-40M. These current ramp rates are still large compared to those typical of tokamaks (1 to 2 MA/s) and are possible in RFPs because of the anomalous penetration of magnetic flux. The slow current ramps of the kind shown are desirable for reactors since the bulk of the flux injection can be supplied directly from the electrical grid at relatively low power, rather than from an expensive on-site energy storage.

A significant decrease in plasma loop voltage is measured upon reversal of the toroidal field and formation of the RFP. This behavior is shown for ZT-40M in Figure 8.5-9, which also shows an optimal value of the pinch parameter from the viewpoint of loop voltage and resistive poloidal-flux consumption. The reduction in resistive flux consumption upon controlling  $\Theta$  at the optimal value is shown in Figure 8.5-10, which gives the resistive

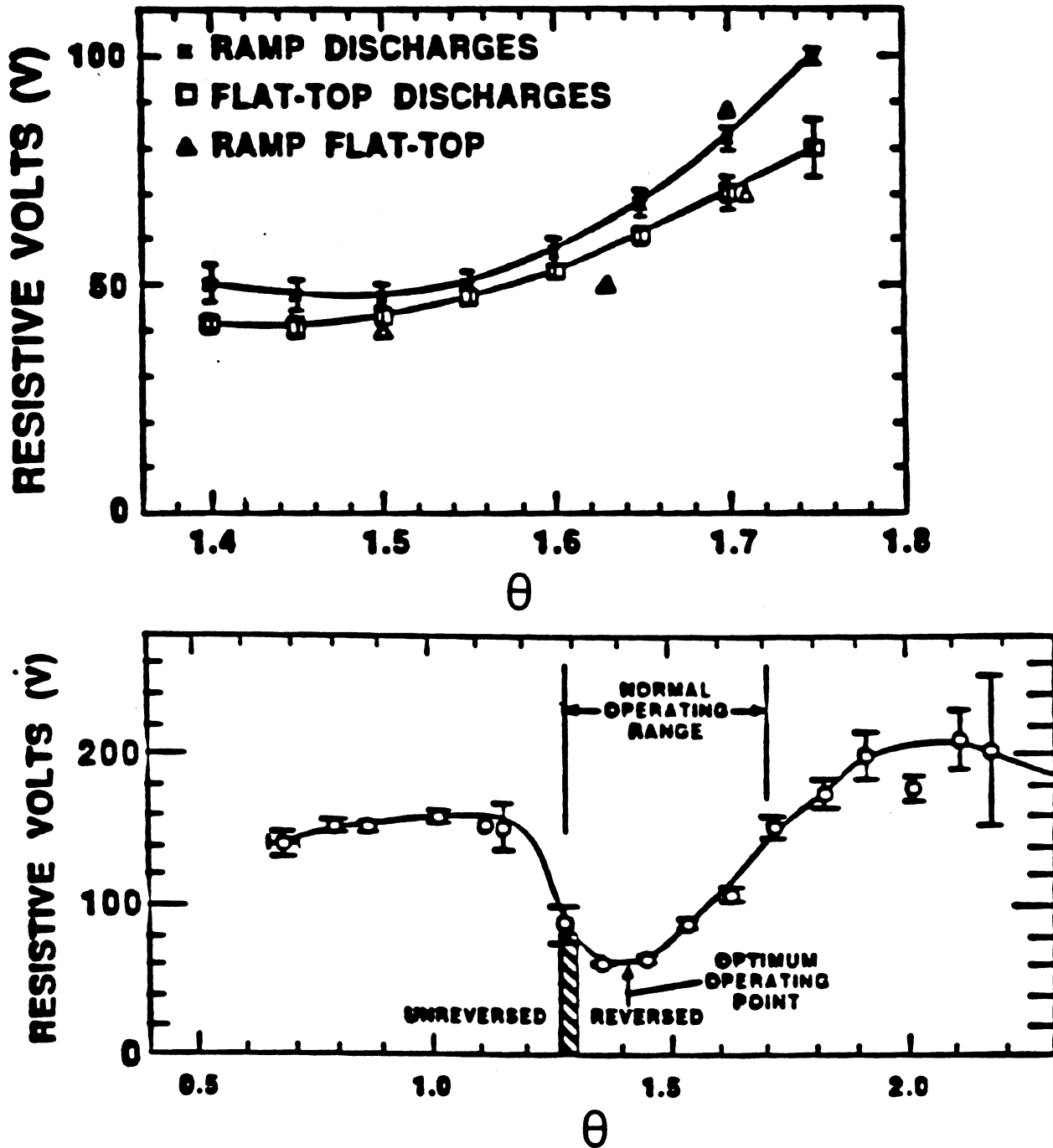


Figure 8.5-9. The dependence of the plasma loop voltage on the pinch parameter upon formation of RFP, showing an optimal value of  $\Theta$  [35].

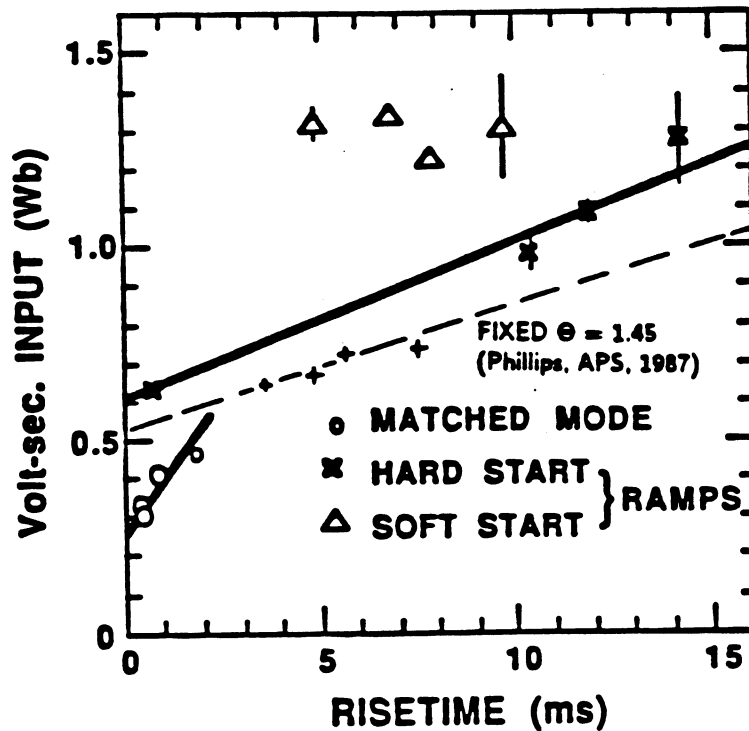


Figure 8.5-10. Dependence of flux input on current risetime for a range of ZT-40M operating conditions [31,35].

volt-second consumption for a range of conditions, including the volt-second efficient matched-mode operation. The ZT-40M data shown on Figure 8.5-10 indicate a constant (resistive) voltage scaling ( $V_{RES} \approx 32.5$  V), which implies that the plasma resistance is decreasing inversely with plasma current in this region. The implication in this scaling on the TITAN-I reactor design is examined in the following section.

### 8.5.3. Reactor Implications

The conditions for plasma breakdown and subsequent RFP formation for the reactor is expected to differ little from the conditions in present and planned RFP experiments [16]. The conditions of the seed-RFP plasma required to start up the TITAN reactor, except for plasma size, are similar to present-day RFP parameters ( $I_\phi = 0.2$ - $0.4$  MA,  $n = 1$ - $2 \times 10^{19} \text{ m}^{-3}$ ,  $T = 0.2$ - $0.4$  eV). Somewhat lower values of  $j_\phi/n$ , however, are desirable for the reactor starting plasma, and better density and impurity control during the  $\sim 10$ -ms breakdown and formation process may be required.

Assuming that the breakdown and formation windows defined for most operating RFP experiments remain unchanged and a seed-RFP plasma of the above-mentioned

characteristics can be provided in larger sizes and longer times, the main physics issue for start-up reduces to one of resistive poloidal-flux consumption during the current ramp-up.

The TITAN start-up scenario includes a fast current ramp to  $I_\phi \simeq 10$  MA (at 3 to 5 MA/s) to rapidly achieve a plasma of reduced resistance. The fast ramp is followed by a slower ramp to ignition and burn,  $I_\phi = 18$  MA (at  $\sim 1$  MA/s). During the current ramp phases, toroidal flux within the TF coil increases from 0.3 Wb to 5.3 Wb (gross) (4.5 Wb, net). This toroidal flux will be supplied by the RFP dynamo through the PF-coil system since the direct injection of the entire toroidal flux at formation would require considerable upgrading of the TF coils and/or considerably increased current ramp rates and is viewed as impractical for the reactor.

The fact that the final plasma state has more toroidal flux than the TF coils alone are capable of supporting, however, must be considered during the current rundown phase of the reactor. For example, if the initial toroidal bias field is  $B_{\phi 0} = 0.1$  T, the initial toroidal flux injected into the reactor torus for a nominal coil radius of  $r_{c\phi} \simeq 1.0$  m is 0.3 Wb ( $\dot{\phi} \simeq 0.3 - 1.0$  kV-turns for  $\tau_{Ro} \simeq 10$  ms). The reversed and plasma toroidal fields at burn conditions are, respectively,  $B_{\phi R} \simeq -0.4$  T and  $\langle B_\phi \rangle = -B_{\phi R}/F \simeq 4.0$  T, which correspond to the respective toroidal fluxes of  $\phi^- \simeq \pi(r_{c\phi}^2 - r_p^2)B_{\phi R} = -0.8$  Wb and  $\phi^+ \simeq \pi r_p^2 \langle B_\phi \rangle = 4.5$  Wb. Hence, the average toroidal field that would result if the plasma suddenly “disappeared” would be  $(\phi^+ + \phi^-)/\pi r_{c\phi}^2 = 1.2$  T or 10 times the initial toroidal field. Furthermore, the net flux change amounts to a field of  $(\phi^+ - \phi^-)/\pi r_{c\phi}^2 = 1.7$  T, which, though not large by tokamak standards, would nevertheless require a structural redesign of the TF coil, and the TF IBC used in the TITAN-I design would also require a reassessment of the start-up power consumption. Lastly, almost all of the final toroidal flux within the plasma,  $\phi^+ \simeq 4.5$  Wb, must be supplied during the current ramp-up by the OH coil through the dynamo. Therefore, if the conversion of poloidal flux to toroidal flux occurs with an efficiency of  $\sim 50\%$ , an additional  $\sim 10$  Wb must be designed into the OH-coil set (an  $\sim 4\%$  effect).

The impact of resistive flux consumption for the reactor during the ramp-up of plasma current is summarized in Table 8.5-I, which compares the experimental (ZT-40M) [35] and TITAN-I ramp-up conditions. The TITAN-I ramp-up conditions require a bipolar OH coil designed for  $\sim 500$ -MWe maximum power from the grid that can supply 247 Wb of inductive poloidal flux and  $\sim 26$  Wb of resistive flux dissipation over the current ramp-up period. The resistive dissipation includes only that deposited in a plasma described by a Spitzer resistivity ( $\eta \propto T^{-3/2}$ ), an appropriate profile factor ( $g_{OHM} = 2.92$  as defined by Equation 3.2-8), and a temperature scaling linearly with current.

Table 8.5-I.

## IMPACT OF RESISTIVE FLUX CONSUMPTION DURING RAMP-UP

	ZT-40M	TITAN-I
<b>Typical Experimental and Reactor Parameters</b>		
Start-up mode	ramp	ramp
Pinch parameter, $\Theta$	1.45 <sup>(a)</sup>	1.5 - 1.6
Plasma current, $I_\phi$ (MA)	0.05 - 0.2	18.
Ramp time, $\tau_R$ (s)	0.015	8.0 <sup>(b)</sup>
Inductive flux, $\phi_{ind}$ (Wb)	$\sim 0.5$	247.
Plasma resistive flux, $\phi_{res}^p$ (Wb)	$32.5 \tau_R$	26.4 <sup>(c)</sup>
Major radius, $R_T$ (m)	1.12	3.9
Minor radius, $r_p$ (m)	0.2	0.6
Geometry factor, $R_T/r_p^2$ (1/m)	28.0	10.6
Final plasma temperature, $T$ (keV)	0.05 - 0.20	10.0
Final loop voltage, $V_\phi$ (V)	32.5	1.9
Plasma ohmic power, $P_{OHM}$ (MW)	6.5	33.6
<b>Resistive Flux Consumption for ZT-40M Scaling (Wb)</b>		
Direct application	–	260.
Corrected for geometry	–	98.4
Corrected for temperature <sup>(d)</sup>	–	54.6
Corrected for temperature and geometry	–	20.1

(a) Optimal (minimum flux consumption) for ZT-40M.

(b) Time to maximum current, almost equilibrium plasma conditions.

(c) Spitzer resistivity,  $Z_{eff} = 1.0 \rightarrow 1.05$ ,  $g_{OHM} = 2.92$ .

(d)  $R_p \propto I_\phi^{-3/2}$ .

The direct application of the “scaling” suggested in Figure 8.5-10 (*i.e.*,  $R_p = 32.5/I_\phi$ ) would give rise to a plasma resistive flux consumption of 260 Wb (Table 8.5-I), almost doubling the volt-second requirement of the OH-coil set from TITAN-I. The TITAN-I design under these conditions would re-optimize at a faster current rise, more massive coils, increased peak (back-biased) power requirement, and possibly higher aspect ratio (to reduce OH-coil stresses in the back-biased condition). Direct application of a geometry correction (*i.e.*,  $R_T/r_p^2$ ) to the ZT-40M resistive volt-second scaling reduces  $\phi_{res}^p$  from 260 Wb to 98 Wb. The assumption of an  $R_p \propto I_\phi^{-3/2}$  (*i.e.*,  $T \propto I_\phi$ ) scaling of the ZT-40M data gives  $\phi_{res}^p = 55$  Wb. Application of both geometry and temperature scalings to the ZT-40M data combine to reduce  $\phi_{res}^p$  to 20 Wb, which is close to the TITAN-I design value of 26 Wb.

In summary, the experimental data base for breakdown and formation is encouraging for direct application to TITAN-I conditions. Extension of the current ramp-up to higher currents and plasmas and to somewhat slower ramp rates (1 to 2 MA/s) is required, and the demonstration of more classical-like scaling of plasma resistance with plasma geometry ( $R_p \propto R_T/r_p^2$ ) and temperature ( $R_p \propto T_e^{-3/2}$ ) is highly desirable. Additionally, the data base for breakdown, formation, and ramp-up should be extended to higher currents and densities, but at lower values of  $\xi = v_D/v_{THe}$ . Active control of density,  $Z_{eff}$ , and equilibrium during start-up is highly desirable.

A broader definition of the RFP formation window is needed as expressed in terms of (1) the minimum  $B_{\phi o}$  as a function of the critical plasma density and/or filling pressure for a given vertical-field error, (2) a minimum  $E_{\phi o}$  for breakdown and impurity burn-through, and (3) a better resolved relationship between  $B_{\phi o}$ ,  $E_{\phi o}$ ,  $P_o$ , and degree of pump-out. Lastly, the ZT-40M scaled loop voltage for TITAN parameters is  $\sim 17$  times that of the estimates using classical-like scaling. Hence, significant reductions are required from the viewpoint of current drive and ohmic power losses (*i.e.*, a factor of 17 increase in  $P_{OHM}$  would make ohmic heating comparable to the alpha-particle heating at steady-state burn conditions).

A number of start-up issues are not expected to be addressed by the next generation of RFP devices, but are of sufficient importance to warrant further analysis. These issues deal with the combined need during the current ramp-up to concurrently initiate equilibrium (including separatrix formation), feedback control, active impurity control, operation of high-heat-flux components, impurity injection to create a highly radiating plasma, pellet injection and density control, and the accommodation of as yet unresolved changes in the heating profiles when the plasma transcends from a predominantly resistively heated entity to one that is heated primarily by charged-particle reaction products.

While these issues cannot be addressed by the RFX and ZTH devices presently under construction, further understanding of these integrated transient effects and the respective plasma responses and associated timing of system responses (*e.g.*, EF-coil control, divertor, impurity injection, fueling, surface cooling) can be developed by additional analytic studies.

## 8.6. SUMMARY AND RECOMMENDATIONS

The performance projected for the TITAN reactor designs depends crucially on the physics areas described in Sections 8.2 through 8.5. Given below are the key physics issues for the high-power-density RFP reactors and recommendations to the RFP experimental physics program.

**Confinement:** Determine spatially resolved profiles in non-transitory RFPs in order to resolve the scaling of intrinsic energy confinement time with plasma geometry, current or current density, and  $F\text{-}\Theta$  value in hot plasmas with low values of  $\xi = v_D/v_{THe}$  and  $Z_{eff}$ . Special emphasis should be placed on investigating radiation-dominated operation and the limits of beta and intrinsic (non-radiative) confinement.

**Current drive:** Investigate both DC and AC techniques for helicity injection in hot RFPs with separatrices and minimal modulation-induced plasma-wall interaction. The impact and management of high levels of reactive power require better resolution. Other means of current drive should also be investigated.

**Impurity control:** Emphasize plasma operation with a toroidal-field separatrix in order to minimize plasma-wall interaction in a highly radiating plasma, eventually leading to high-recycling divertor operation and an easing of OFCD with a fixed separatrix position.

**Formation and start-up:** Clearly resolve the scaling of plasma resistance with current ramp rate, current, geometry, and  $F\text{-}\Theta$  values in plasmas with low values of electron streaming parameters, and minimal and/or controllable plasma-wall interactions.

Clearly, these key issues and the conditions needed and/or assumed for the compact RFP reactor designs are interrelated and symbiotic. The existence and role of a close-fitting electrically conducting shell that surrounds the RFP has strong impact on these

physics issues. Hence, as a fifth, but highly integrating recommendation: resolve the need for and characteristics of a conducting shell with electrical breaks on the formation and start-up, confinement, current drive, and impurity control which represent at present an inadequately mapped issue for the RFP. This is an issue that the TITAN study circumnavigated numerous times in its overall quest to resolve physics and engineering-systems issues for cost-effective and technologically attractive, high-power-density fusion reactors.

Finally, current termination is a safety and economics concern because of the large magnetic stored energy in the TITAN plasma. Experimental techniques for control of current termination and plasma shutdown, leading to a "soft-landing," especially by passive means, are essential for achieving a high degree of safety and environmental attractiveness for RFP reactors.

**REFERENCES**

- [1] F. Najmabadi, N. M. Ghoniem, R. W. Conn, *et al.*, "The TITAN Reversed-Field Pinch Reactor Study, Scoping Phase Report," joint report of University of California Los Angeles, General Atomics, Los Alamos National Laboratory, and Rensselaer Polytechnic Institute, UCLA-PPG-1100 (1987).
- [2] R. W. Conn (chairman and editor), "Magnetic Fusion Advisory Committee Panel X Report on High Power Density Fusion Systems" (May 8, 1985).
- [3] J. Sheffield, R. A. Dory, S. M. Cohn, J. G. Delene, L. F. Parsley, *et al.*, "Cost Assessment of a Generic Magnetic Fusion Reactor," Oak Ridge National Laboratory report ORNL/TM-9311 (1986) 103.
- [4] R. A. Krakowski, R. L. Miller, and R. L. Hagenson, "The Need and Prospect for Improved Fusion Reactors," *J. Fusion Energy* **5** (1986) 213.
- [5] R. A. Krakowski, R. L. Hagenson, N. M. Schnurr, C. Copenhaver, C. G. Bathke, R. L. Miller, and M. J. Embrechts, "Compact Reversed-Field Pinch Reactors (CRFPR)," *Nucl. Eng. Design/Fusion* **4** (1986) 75.
- [6] H. A. Bodin, R. A. Krakowski, and O. Ortolani, "The Reversed-Field Pinch: from Experiment to Reactor," *Fusion Technol.* **10** (1986) 307.
- [7] R. L. Hagenson, R. A. Krakowski, C. G. Bathke, R. L. Miller, M. J. Embrechts, *et al.*, "Compact Reversed-Field Pinch Reactors (CRFPR): Preliminary Engineering Considerations," Los Alamos National Laboratory report LA-10200-MS (1984).
- [8] C. Copenhaver, R. A. Krakowski, N. M. Schnurr, R. L. Miller, C. G. Bathke, *et al.*, "Compact Reversed-Field Pinch Reactors (CRFPR)," Los Alamos National Laboratory report LA-10500-MS (1985).
- [9] P. Thullen and K. Schoenberg (Eds.), "ZT-H Reversed-Field Pinch Experiment Technical Proposal," Los Alamos National Laboratory report LA-UR-84-2602 (1984) 26.
- [10] G. Malesani and G. Rostagni, "The RFX Experiment," *Proc. 14th Symp. Fusion Technology*, Avignon (1986) 173.
- [11] Y. Hirano, T. Shimada, Y. Maejima, and K. Ogawa, "Improved Stability Period in High-Current-Density Operation of Reversed-Field Pinch of ETL-TPE-1R(M)," *Nucl. Fusion* **22** (1982) 1613.

- [12] B. Alper *et al.*, "RFP Confinement Studies in ETA-BETA-II," *Proc. 12th European Conf. on Cont. Fusion and Plasma Phys.*, Budapest, Hungary (September 1985), *European Phys. Soc.* **1** (1985) 578.
- [13] H. A. B. Bodin, "New Results from the HBTX Experiment," *Bull. Am. Phys. Soc.* **32** (1987) 1784.
- [14] T. Tamano, W. D. Bard, T. N. Carlstrom, C. Chu, B. Curwe, R. K. Fisher, *et al.*, "High Current, High Beta Toroidal Pinch Experiment in OHTE," in *Proc. 10th Int. Conf. on Plasma Phys. and Cont. Nucl. Fusion Res.*, London, U. K. (September 1984), IAEA, Vienna (1985).
- [15] D. A. Baker, C. J. Buchenauer, L. C. Burkhardt, E. J. Caramana, J. N. DiMarco, J. N. Downing, *et al.*, "Experimental and Theoretical Studies of the ZT-40M Reversed-Field Pinch," in *Proc. 10th Int. Conf. on Plasma Phys. and Cont. Nucl. Fusion Res.*, London, U. K. (September 1984), IAEA, Vienna (1985).
- [16] D. B. Thomson (Ed.), *Proc. Int. Workshop on Engineering Design of Next Step Reversed Field Pinch Devices*, Los Alamos National Laboratory (July 13-17, 1987).
- [17] C. G. Bathke, R. A. Krakowski, R. A. Krakowski, and R. L. Miller, "A DT Neutron Source Based on the Reversed Field Pinch," *Proc. 12th IEEE Symp. on Fusion Eng.*, Monterey, CA (October 1987) 829.
- [18] M. K. Bevir and J. W. Gray, "Relaxation, Flux Consumption and Quasi Steady State Pinches," *Proc. of RFP Theory Workshop*, Los Alamos, NM, U. S. A. (1980), Los Alamos National Laboratory report LA-8944-C (1982) 176.
- [19] K. F. Schoenberg, J. C. Ingraham, C. P. Munson, *et al.*, "Oscillating-Field Current-Drive Experiments in a Reversed-Field Pinch," *Phys. Fluids* **8** (1989) 2285; also R. A. Scardovelli, R. A. Nebel, and K. A. Werley, "Transport Simulation of the Oscillating Field Current Drive Experiment in the Z-40M," Los Alamos National Laboratory report LA-UR-2802 (1988).
- [20] R. S. Massey, R. G. Watt, P. G. Weber, G. A. Wurdien, D. A. Baker, C. J. Buchenauer, *et al.*, "Status of the ZT-40M RFP Experimental Program," *Fusion Technol.* **8** (1985) 1571.
- [21] P. G. Weber *et al.*, "Results from the Los Alamos RFP Experiments," *Proc. 12th European Conf. on Cont. Fusion and Plasma Phys.*, Budapest, Hungary (September 1985), *European Phys. Soc.* **1** (1985) 570.

- [22] M. M. Pickrell, J. A. Phillips, C. J. Buchenauer, T. Cayton, J. N. Downing, A. Haberstich, *et al.*, "Evidence for a Poloidal Beta Limit on ZT-40M," *Bull. Am. Phys. Soc.* **29** (1984) 1403.
- [23] R. Hancox, R. A. Krakowski, and W. R. Spears, "The Reversed-Field Pinch Reactor Concept," *Nucl. Eng. and Res.* **63** (1981) 251.
- [24] K. F. Schoenberg, J. C. Ingraham, C. P. Munson, P. G. Weber, D. A. Baker, R. F. Gribble, *et al.*, "Oscillating-Field Current Drive Experiment in ZT-40M Reversed Field Pinch," Los Alamos National Laboratory report LA-UR-88-122, submitted to *Phys. Fluids* (1988).
- [25] R. L. Hagenson and R. A. Krakowski, "The Spheromak as a Compact Fusion Reactor," Los Alamos National Laboratory report LA-10908-MS (March 1987).
- [26] C. G. Bathke and R. A. Krakowski, "A Comparison Study of Toroidal-Field and Bundle Divertors for a Compact Reversed-Field Pinch Reactor," *Fusion Technol.*, **8** (1985) 1616.
- [27] A. K. Prinja and R. W. Conn, "An Axially-Averaged Radial Transport Model of Tokamak Edge Plasmas," *J. Nucl. Mater.* **128-129**, (1984) 135.
- [28] A. F. Almagri, *et al.*, "Reversed Field Pinch Experiments with Various Boundary Conditions," in *Proc. Int. School of Plasma Phys. Course and Workshop on Physics of Mirrors, Reversed-Field Pinches, and Compact Tori*, Varenna, Italy (September 1987).
- [29] T. R. Jarboe and B. Alper, "A Model for Loop Voltage of a Reversed-Field Pinch," *Phys. Fluids* **30** (1987) 1177.
- [30] A. Kellman, E. Lazzaro, P. Noll, F. C. Schveller, and P. Thomas, "Breakdown Conditions in JET," *Bull. Am. Phys. Soc.* **30** (1985) 1524.
- [31] J. A. Phillips, L. C. Burkhardt, A. Haberstich, R. B. Howell, J. C. Ingraham, E. M. Little, K. S. Thomas, and R. G. Watt, "ZT-40M Current Risetime Study," Los Alamos National Laboratory report LA-9717-MS (1983).
- [32] F. Engelmann, N. Fujisawa, B. B. Kadomtsev, V. I. Pistunovich, J. A. Schmidt, and M. Sugihara, "Physics Design Basis," in *International Tokamak Reactor, Phase One*, IAEA, Vienna (1982) Chap. III, p. 127.

- [33] R. G. Watt and J. N. Downing, "Pre-ionization Studies in ZT-40M," Los Alamos National Laboratory report LA-9163-MS (February 1982).
- [34] J. A. Phillips, Los Alamos National Laboratory, private communication (August 1986).
- [35] J. A. Phillips, D. A. Baker, R. F. Gribble, and C. Munson, "Start-up of Reversed-Field Pinches and Current Ramping Using Dynamo Action," submitted to *Nucl. Fusion* (1987).
- [36] G. A. Wurden, P. G. Weber, R. G. Watt, C. P. Munson, T. E. Cayton, and K. Buchl, "Refueling and Density Control in the ZT-40M Reversed-Field Pinch," in *Proc. Int. School of Plasma Phys. Course and Workshop on Physics of Mirrors, Reversed-Field Pinches, and Compact Tori*, Varenna, Italy (September 1987).